THESIS FOR THE DEGREE OF DOCTOR OF PHILOSOPHY

# Simulation of the Melting and Cooling of Palladium Clusters

Jan Westergren



Department of Experimental Physics
Chalmers University of Technology and Göteborg University
Göteborg, Sweden 2001

Simulation of the Melting and Cooling of Palladium Clusters
JAN WESTERGREN
ISBN 91-7291-084-4



Doktorsavhandlingar vid Chalmers tekniska högskola
Ny serie nr 1767
ISSN 0346-718X

Department of Experimental Physics
Chalmers University of Technology and Göteborg University
412 96 Göteborg
Sweden
Telephone +46 (0)31 - 772 10 00

Chalmers Reproservice
Göteborg, Sweden 2001

Till Marie,
Rasmus och Sofia

**Simulation of the Melting and Cooling of Palladium Clusters**

JAN WESTERGREN
Department of Experimental Physics
Chalmers University of Technology and Göteborg University

## Abstract

The thermal behaviour of palladium clusters has been investigated using Monte Carlo simulation in various ensembles. Furthermore the energy transfer between palladium clusters and rare gas atoms has been calculated in simulated collisions aiming for a calculation of the cooling of clusters in a rare gas atmosphere. The internal structure of the cluster has been modeled by a Many-Body Alloy potential and the interaction between cluster and rare gas atom has been modeled by the Lennard-Jones potential. At melting, the cluster frequently switches from one phase to the other in the case of $Pd_{13}$. However, due to a free energy phase barrier, the simulations are quasiergodic and the simulation results are not reliable within the phase coexistence region for $Pd_{54}$, $Pd_{55}$, $Pd_{147}$ and $Pd_{309}$. In contrast to bulk, the clusters up to $Pd_{147}$ (and possibly $Pd_{309}$) show a distinct two-state behaviour and cannot be partially molten. The coexistence of the phases is instead over time or over an ensemble of clusters. The geometric properties of the clusters change at melting. For instance, the icosahedral clusters change to an on average non-spherical shape at melting. The simulation results are compared for the canonical and microcanonical ensembles as well as for constant temperature molecular dynamics simulations. The agreement between the three methods is good.

Simulations are also performed to calculate the density of states of separated solid and molten isomers. The Reference System Equilibration method proved to accurately reproduce the density of states of anharmonic systems. However, in order to estimate the melting point of a cluster, density of states calculations must be complemented by a knowledge of the number of statistically equivalent molten isomers.

In the second part of the thesis, collisions between $Pd_{13}$ and rare gas atoms are considered. The collisions are simulated by molecular dynamics simulation. The energy transfer data obtained in the simulations were used to calculate the cooling of the cluster in a rare gas atmosphere. Furthermore, the character of the collisions was studied. At low gas temperatures, multiple encounters and even sticking were observed. By statistical models, like the Partially Ergodic Multiple Encounter Theory, energy transfer efficiency was investigated as a function of cluster and gas temperatures as well as of the kind of gas atom.

**Keywords**: metal clusters, melting, density of states, phase barrier, collision, energy transfer, sticking, cooling

# List of Papers

This thesis is based on the following papers, referred to by Roman numerals in the text:

**Paper I** **Melting of palladium clusters - Canonical and microcanonical Monte Carlo simulation**
Jan Westergren, Arne Rosén and Sture Nordholm
J. Chem. Phys., submitted

**Paper II** **Melting of palladium clusters - Density of states determination by Monte Carlo simulation**
Jan Westergren and Sture Nordholm
J. Chem. Phys., submitted

**Paper III** **Noble Gas Temperature Control of Metal Clusters: A Molecular Dynamics Study**
Jan Westergren, Henrik Grönbeck, Seong-Gon Kim and David Tománek
J. Chem. Phys., **107**, 3071 (1997)

**Paper IV** **Statistical Theory of Cluster Cooling in Rare Gas - I. Energy Transfer Analysis for Palladium Clusters in Helium**
Jan Westergren, Henrik Grönbeck, Arne Rosén and Sture Nordholm
J. Chem. Phys., **109**, 9848 (1998)

**Paper V** **Molecular Dynamics Simulation of Metal Cluster Cooling and Heating in Noble Gas Atmosphere**
Jan Westergren, Henrik Grönbeck, Arne Rosén and Sture Nordholm
NanoStructured Materials Vol **12**, 281 (1999)

**Paper VI** **Cooling efficiency in collisions between $Pd_{13}$ and He, Ne, Ar and Kr**
Jan Westergren, Sture Nordholm and Arne Rosén
Eur. J. Phys. D, submitted

**Paper VII** **Statistical Theory of Cluster Cooling in Rare Gas - II. The PEMET model**
Jan Westergren, Sture Nordholm and Hongrei Li
Physical Chemistry Chemical Physics, submitted

Related work but not included in this thesis:

**On the role of density fluctuations in the equation of state of a simple fluid**
Jan Westergren, Sture Nordholm and Robert Penfold
Mol. Sim., **27**, 17 (2001)

# Contents

# Chapter 1

# Introduction

## 1.1 Preface

Smaller and smaller building blocks are used in materials science in order to be able to design materials so that precise properties are obtained. One of the objects that draw attention in this search for optimal materials is clusters and particularly metal clusters [1, 2, 3, 4, 5, 6]. A metal cluster consists of a number of metal atoms that are bound together in an aggregate. They can be thought of as an intermediate between the single atom and metal bulk material. The scientific field of cluster research is indeed a vivid one. In cluster research the properties of clusters as for instance stability [7, 8, 9], ionization potentials, reactivity with gases, and magnetic properties are investigated. Like bulk material, the cluster properties depend on parameters as elemental constitution, geometric and electronic structure and temperature [10]. In addition the cluster properties depend on the number of atoms in the cluster. It was discovered that cluster properties like the ionization potential [11] does not evolve gradually from small clusters to large clusters but exhibit an irregular dependence on cluster size. It might be intuitive that properties can change dramatically when one atom is added to a cluster of say ten atoms. But that the melting point is alternating with sodium cluster size in the region 100 - 200 atoms is not beforehand obvious [12]. When properties of the aggregated atoms do not change any more with size, the aggregate does not form a cluster any more. In practise, most clusters investigated in the literature consist of less than 1000 atoms.

In transition metal clusters, among which we found the palladium clusters, the coordination number of the surface atoms is much less than in bulk. Therefore, two metal cluster readily combine to form a larger cluster. This property makes them difficult to handle. For instance, free clusters cannot be studied in an ordinary gas, since the collisions with each other and with walls would ruin the initial size distribution. Free clusters are instead often studied in cluster beam experiments. Moreover, clusters are often studied when deposited on a substrate [13, 14, 15, 16]. Although, the clusters have not yet been put to technological use, there are areas where they are promising.

Two areas in close connection to cluster research are catalysis [17, 18, 19] and computer information storage [20, 21, 22, 23].

In cluster experiments it was observed that many properties of free clusters depend on the internal cluster temperature. Among these properties we find the ionization potential [24, 25, 26], reactivity [27] and magnetic moments [10]. Hence, the thermal properties of clusters are of great interest. In nowadays famous experimental work of the group at Universität Freiburg in Germany, the melting of sodium clusters was investigate [12, 28, 29]. In their method, size-selected clusters assume a desired temperature by passing a heat bath of rare gas. Subsequently, a photofragmentation pattern is recorded. The temperature of the clusters can be increased either by injecting a known amount of photon energy after the heat bath or by increasing the heat bath temperature. When the photofragmentation patterns match, the photon energy corresponds to the temperature increase and the heat capacity can be calculated.

A heat bath has also been used by Chandezon *et al.* [8]. In an experiment where sodium clusters were allowed to evaporate, the relative stability of the cluster sizes was investigated. By letting the clusters evaporate in a heat bath instead of in vacuum, a more strongly modulated cluster size distribution was obtained and thus the shell effects of sodium clusters appeared more clearly.

Melting of clusters was also observed by von Pietrowski *et al* [30]. They studied melting of Ne clusters by doping them with Xe atoms. The spectrum of excited xenon atoms was measured by fluorescence excitation spectroscopy. The observed spectral shift is proportional to the number of nearest neighbours and they could conclude that the Xe atoms were surrounded by Ne atoms, i.e. the Xe atoms had penetrated the cluster which proved the presence of a molten phase of the cluster. Heinze *et al.* [31] have derived a method to convert experimental data on scattering from a cluster into the mean kinetic energy, i.e. the temperature. In early experimental work of Buffat and Borel [32] and Iijima and Ichihashi [33] structural changes corresponding to a molten phase were observed in electron microscope.

When I joined the Molecular Physics Group in Göteborg, an experimental setup using the laser vapourization technique was used to study reactivity of free metal clusters. One issue was to investigate the dependence of the reactivity on cluster temperature. The question arose whether the number of collisions between the clusters and the surrounding gas was sufficiently large to control the cluster temperature? And what kind of gas would cool the clusters must efficiently? By means of molecular dynamics simulation of collisions between a gas atom and a cluster we tried to answer these questions. However, in order to calculate the cooling of the cluster the heat capacity must be known. In the beginning of our work we used the results from a work by my coworker Henrik Grönbeck [34] and others. They used molecular dynamics simulation with the Nosé-Hoover thermostat [35]. In order to investigate whether different simulation techniques would give different results we also calculated the cluster heat capacity using Monte Carlo simulation.

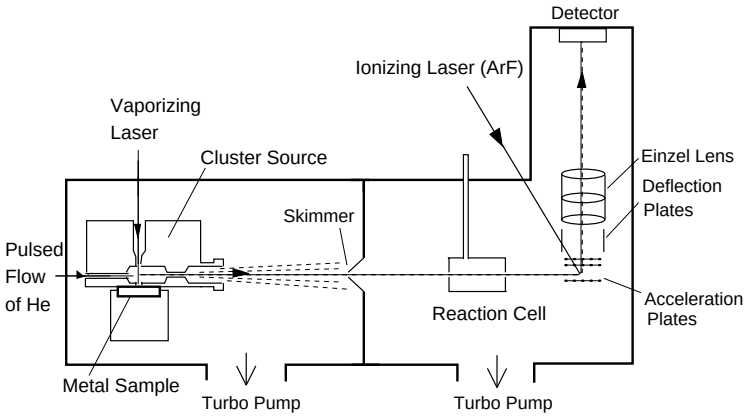


Figure 1.1: The experimental set-up for cluster production using the laser vapourization technique. The figure is drawn by Lotta Holmgren [42].

Previously in our group, theses on clusters have been presented by Bo Wästberg [36], Mats Andersson [37], Daniel Östling [38], Henrik Grönbeck [39], Lotta Holmgren [40] and Thorbjörn Åklint [41].

## 1.2 The laser vaporization technique

In the early 1980s the laser vaporization technique [43, 44] became available and made experimental study of free clusters practicable. This technique has been used in our group the last ten years for the investigation of cluster reactivity [45]. The set-up for cluster production is found in Fig. 1.1. In a chamber called the cluster source, a pulsed laser beam is focused onto a metal target and vapourizes surface metal atoms. The metal vapour formed is entrained in a pulsed flow of carrier gas. In collisions with the carrier gas the metal atoms are cooled and may condense into clusters. In order to study how the clusters act as a function of temperature the cluster source is either at room temperature or at liquid nitrogen temperature, 77 K. Before the clusters leave the source they may collide with each other, forming bigger clusters. After passing the nozzle the atoms and clusters undergo a supersonic expansion into vacuum and the clusters form a beam. In the expansion the cluster growth is interrupted and the clusters range in size from one atom to several hundred atoms. Before entering the reaction cell, most of the carrier gas is skimmed off by a skimmer. Passing through the reaction cell, the clusters experience a low number of collisions with reactive molecules, e.g. CO. The reactivity is evaluated by time-of-flight spectrometric detection of the relative abundance of bare and reacted clusters.

## 1.3 Melting of clusters

The thermodynamical properties of clusters may help the understanding of processes in bulk. A great deal of effort has been put into the analysis of melting of clusters. It is remarkable that the research was initiated by computer simulations rather than experimental work. Early simulations were performed by e.g. Kaelberer and Etters [46] and Lee *et al.* [47] in the 1970s. Since the late 1980s, scientists have formulated theories for the thermal behaviour of clusters [48, 49, 50]. Much progress has been made in statistical thermodynamics of finite systems. It has been found that some thermodynamical laws have to be slightly reinterpreted when the system is finite. For instance, such fundamental concept as the melting temperature has to be changed into a melting temperature interval for clusters. Over the last 15 years many scientist have done similar simulations of melting as will be presented in this thesis. Our results do agree with the common knowledge established in the literature. In **Paper II**, the Reference System Equilibration method is used in order to contribute to the solution of one of the major problems in the simulation of condensed matter: the prevention of phase crossing by free energy barriers.

## 1.4 Cooling and collisions

Molecular collisions are most important events in chemistry. By collisions gas phase reactions are initiated. By collisions reactants can be cooled and stabilized [51]. Also in physics collisions are crucial. Adsorption, desorption and sticking of molecules on surfaces are two examples within surface physics where collisional energy transfer is of importance [52, 53].

Two major areas of collisional investigations might be mentioned. The first one is bimolecular collisions. One of the simplest chemical reactions is the gas-phase unimolecular reaction. In such a reaction the reactant and the product maybe the same molecule, with a modification of for instance the structure in an isomerization reaction. In early studies of such reactions, Lindemann [54] showed that the reactant needs to be energetically activated in a collision in order to transform into products. In the RRKM theory [55] the collisional energy transfer is one of the ingredients needed to calculate the reaction rate and this has been one reason for measuring/calculating the energy transfer rate [56, 57].

A second major area of collision investigations is that of molecule-surface collisions [58, 59, 60, 61]. In cluster research cluster-surface collisions are of ultimate interest. In the last years deposition of clusters on substrates has become one of the major issues in cluster research. There is a wealth of studies of collisions of clusters on surfaces [14, 15, 62, 63, 64, 65, 66, 67, 68, 69, 70, 71] (see also the proceedings of ISSPIC 1998 [72]). Cluster-surface collisions have, however, also been used to understand collision induced cluster reactions [73]

and charging of scattered water clusters [74]. Simulations of cluster-cluster and cluster-molecule collisions may be found in Ref. [75, 76, 77, 78, 79].

For a long time the collisional energy transfer was deduced from results of "indirect methods" like reaction studies [51, 80]. The most common experimental set-up for studying chemical reaction dynamics has been molecular crossed beam experiments for which Dudley Herschbach and Yuan Lee were awarded the Nobel Prize in chemistry in 1986 [81]. This technique has also been used for dissociation of sodium clusters [82]. Since the late 1980s "direct" spectroscopic methods have been used to measure the energy transfer. In these methods the excitation of the molecules is measured [51].

With computer simulations the problem is put in a different light. By integrating the trajectories of the atoms the energy transfer can be calculated directly. The drawback is of course that the exact interaction between the colliding species is not known and hence the simulations need experimental confirmation. Still, even if the simulation may not be capable of exactly reproducing experimental data, it is an invaluable tool for investigation of collision phenomena and trends. For instance, the variation of the energy transfer can be investigated for varying interspecies potential at fixed masses. Such an investigation is difficult in experiments.

The gain in knowledge from one specific trajectory is minor, especially since the interaction between the atoms is not precisely in agreement with experimental reality. Recently, trajectories have been integrated with the forces calculated by *ab initio* methods [83]. However, the number of collisions that are required to obtain an acceptable accuracy in the average energy transfer is so large that *ab initio* methods must be left to the future.

The outcome of a specific trajectory is chaotic. The slightest change in initial conditions and the trajectory will become totally different. The average behaviour is however stable. As an example we recall that when changing the compiler for our simulation program, the incoming gas atom often went a totally different way in the collisions, despite identical input. For the *average* energy transfer, on the other hand, the outcome was independent of compiler.

Although the trajectories are chaotic we have been able to see some trends. It might seem intuitive that gas atoms heading towards a cluster with a small impact parameter bounce off while gas atoms with a larger impact parameter can pass the cluster with a net attraction only. But that the former class of trajectories heats the cluster and the later one cools the cluster, although the gas and cluster are in thermal equilibrium, might be surprising (see Fig. 7.1). Single trajectories might also give insight into the sticking phenomenon. Still, it is the average behaviour that is of major interest.

Thermodynamics predicts that the average energy transfer should be from warmer to colder species. We can thus write the energy transfer from species A to B as

$$\langle \Delta E \rangle = k \langle T_A - T_B \rangle . \tag{1.1}$$

The factor $k$ may however vary with the temperatures $T_A$ and $T_B$. One of the first attempts to model the energy transfer was the Strong Collision Assumption proposed by Hinshelwood [84]. In this model he proposed that an excited species was cooled to equilibrium with the surrounding atmosphere after only one collision. This model considerably overestimated the energy transfer efficiency. Tardy and Rabinovitch [85] and Hippler and Troe [51] showed that the typical energy transfer collision is weak rather than strong. In this theses we will use three statistical models to describe the energy transfer: the Ergodic Collision Theory (ECT) [86], the Partially Ergodic Collision Theory (PECT) [87, 88] and the Partially Ergodic Multiple Encounter Collision Theory (PEMET) [87, 88].

The original aim for the collision simulations was to study the cooling of clusters, especially at the aggregation of the clusters. By means of simulations we have calculated the temperature decay of hot $Pd_{13}$ in various atmospheres of rare gases. For this calculation, only the energy transfer results from collision simulations and the heat capacity data (from the MC simulations) are required. The project was however extended to statistical treatment with ECT, PECT and PEMET in order to better understand the underlying dynamics of the collisions.

# Part I

# Melting of palladium clusters

# Chapter 2

# Internal cluster structure

The reliability of the computational and simulation results are naturally highly dependent on the choice of model to describe the electronic structure of the cluster. Only clusters in their electronic ground state are considered in this work and thus only the vibrations and rotations of the cluster contribute to the properties. Since it is the potential energy surface that causes the vibrations, the electronic structure need to be known for the electronic ground state. The quality of the model must however be balanced against computational effort. The results presented in this thesis are based upon approximately 10 billion computations of the potential energy of cluster configurations and 5 million collision trajectories. Even though the simulations in some cases could have been shortened, the computers of today are too slow to manage so many calculations using *ab initio* techniques. Model Hamiltonians must be used. The properties that must be realistically modeled are for the melting calculations: the cohesive energy, the geometric structure, the normal mode frequencies and the anharmonicity of the vibrations. In the simulations we have used the Many-Body Alloy potential developed by Tománek *et al.* [89]. This potential is also known by the name Gupta potential [90].

Palladium is a transition metal with the free atom electron structure $(\mathrm{Kr})4\mathrm{d}^{10}$, i.e. the d shell is filled. However in the form of cluster or bulk, the configuration tends to be more like $(\mathrm{Kr})4\mathrm{d}^{9}5\mathrm{s}^{1}$ [91]. In the MBA potential the cohesive energy is the sum of a many-body attractive part and a pairwise repulsive part. The repulsive part is due to the coulombic repulsion of the ion cores and the Pauli repulsion of the overlapping s orbitals [39] and it is modeled as being of Born-Mayer type, i.e. the repulsion decays exponentially with the separation $r_{ij}$ between atoms $i$ and $j$:

$$\epsilon_0 \sum_{j \neq i} \exp\left(-p\left(r_{ij}/r_0 - 1\right)\right). \tag{2.1}$$

The attractive part is based on the second moment approximation of tight-binding calculations. The attraction is due to hybridization of the d states into bands when the free atoms are brought together into a crystal. The

binding energy is obtained by an integration over the occupied states

$$E_{bond}(i) = \int_{-\infty}^{E_f} \left(E - E'\right) \Omega_i(E)\, dE, \tag{2.2}$$

where $E_f$ is the Fermi energy, $E'$ is the energy of the centre of the band and $\Omega_i(E)$ is the local density of states near atom $i$. If we consider only interaction between nearest neighbours $i$ and $j$, the binding energy of atom $i$ is proportional to the square root of the sum of "hopping" integrals which furthermore can be assumed to have an exponential decay:

$$E_{bond}(i) \propto \left(\sum_j \langle \varphi_i | H | \varphi_j \rangle\right)^{1/2} \propto \left(\sum_j e^{-2qr_{ij}}\right)^{1/2}. \tag{2.3}$$

The bonding and repulsive parts are now fused into the MBA expression for the total potential energy

$$U = \sum_{i=1}^{n} \left( -\xi_0 \sqrt{\sum_{j \neq i} \exp\left(-2q\left(r_{ij}/r_0 - 1\right)\right)} + \epsilon_0 \sum_{j \neq i} \exp\left(-p\left(r_{ij}/r_0 - 1\right)\right) \right). \tag{2.4}$$

The parameters that we have used were calculated [89] by fitting the energy versus lattice parameter to density functional theory (DFT) calculations of totally frozen bulk palladium with the local density approximation (LDA). The resulting parameters are $\xi_0 = 1.2630$ eV, $\epsilon_0 = 0.08376$ eV, $r_0 = 2.758$ Å, $p = 14.8$ and $q = 3.40$. These parameter values were also used in the work by Grönbeck [34] with which we are going to compare our melting simulations. This parameterization has proved to compare favourably with SCF-CI calculations of optimized geometric structures of $Pd_{13}$ [92]. The MBA predicts the radius of $Pd_{13}$ to be 2.50 Å and the energy difference between the icosahedral and the octahedral structures to be 0.12 eV. The SCF-CI calculations resulted in 2.60 Å and 0.12 eV, respectively. The use of a many-body potential can be crucial for metallic systems. Many properties, like stacking fault energies, surface structure and relaxation cannot be properly described by pair-potentials [93]. The MBA potential has been used for metallic bulk and metal clusters by many others [93, 94, 95]. Other potentials that have been used for metallic systems are for example the Embedded-Atom Method [96] and the Effective Medium Theory [97]

Jarrold and Bower proposed a model for the vibrational spectrum of metal clusters [98]. In this model, the density of modes is supposed to be proportional to $\omega^2$ but vanish above a cut-off frequency. Here $\omega$ is the angular frequency. The cut-off frequency for a cluster with $n$ atoms is assumed to be given by

$$\omega_{cut-off}(n) = \omega_{cut-off}(\infty) \cdot \left(1 - n^{-0.33}\right)^a, \tag{2.5}$$

where $a$ is an empirical parameter. The cut-off frequency for bulk is obtained from the Debye temperature [99],

$$\omega_{cut-off}(\infty) = \frac{2\pi k_B \theta_{Debye}}{h}. \tag{2.6}$$

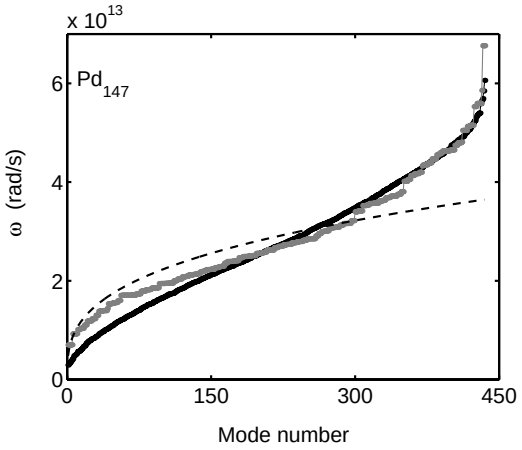


Figure 2.1: The angular frequencies of the solid (black) and molten (grey) isomers at 0 K. The dashed line represents Jarrold's model. The number of normal modes are 435 for $Pd_{147}$.

For palladium, $\theta_{Debye} = 275$ K and the frequency of $Pd_2$ is 210 $cm^{-1}$ [100]. Now $a$ can be calculated and finally the frequency spectrum of $Pd_{147}$ clusters. In Fig. 2.1, the spectrum according to Jarrold's model is drawn as the dashed curve. The black and grey dots are the frequencies from a normal mode analysis using the MBA potential for the solid $Pd_{147}$ and the supercooled molten $Pd_{147}$ (see Sec. 5.3), respectively. The Jarrold model and the MBA potential model are in fair, although not excellent agreement.

The agreement of the lattice constant is good, but, unfortunately, the parameters do not reproduce the experimental cohesive energy of bulk Pd. The parameters that we have used predict the cohesive energy per atom to be $-3.47$ eV to be compared with the experimental value $-3.89$ eV [99]. This error will definitely affect the melting point calculations, as the melting point is proportional to the cohesive energy, all other parameters being fixed. But since we had started with these parameters, we have used them throughout the work. The parameters by Cleri and Rosato [93] and Rey *et al.* [94] will certainly describe at least the bulk properties of palladium better. Still, our parameters reproduce the volume expansion of bulk palladium fairly well. In Fig. 5.10, the volume per particle at zero pressure from Monte Carlo simulations is compared with experimental data [101]

Metal clusters with special numbers of atoms, so-called magic numbers, have proven to be more stable than others [102]. Such stable clusters often have an electronic or geometric closed shell. The icosahedral clusters with 13, 55, 147, 309, ... atoms are examples of clusters with closed geometric shells [103]. The reason small clusters take another crystallographic shape than bulk is that the surface is rearranged to lower surface energy. The rearrangement introduces an internal strain but still the total energy is lowered [104]. One important property of the icosahedral clusters is that they prob-

ably have a unique minimum energy configuration. Tsai and Jordan [105] performed a search for the 30 isomers with lowest energy in $LJ_{13}$ and found that the icosahedral isomer had a considerably lower energy than the other isomers . In contrast, for the non-icosahedral cluster $Pd_{34}$ we found that many minima are close to the global minimum energy.

# Chapter 3

# Phases and phase transitions

## 3.1 Bulk systems

Phases and phase transitions of bulk fluids and solids have been observed at least as long as man has been able to boil water. In Sweden the melting of ice in the spring is eagerly awaited each year. Phase transitions have also been put to technological use for a long time. The most obvious phases, solid, liquid and gas, can easily be characterized by eye. However, the solid phase can be divided into many subphases where the atomic structure varies, resulting in different properties. One example is the different phases of ice [106]. At high pressures ice can attain different crystal structures with for instance different compressibility.

The formal definition of a phase is given in standard textbooks, e.g. [107]

> A state of matter that is uniform throughout, not only in chemical composition but also in physical state.

The phases and phase transitions are beautifully explained by thermodynamics. Here I will give a short review of the thermodynamics of phase transitions essentially following "Thermodynamics and an introduction to thermostatics" by H. B. Callen [106]. The system is assumed to consist of one kind of atoms only. Depending on what parameters that are fixed for a system, (e.g. the volume (V), number of atoms (N) pressure (P) and temperature (T)), different thermodynamical potentials determine the equilibrium state. At constant N,T,V, the equilibrium is the state with minimal Helmholtz free energy, $F = E - TS$. $E$ is the internal energy, $S$ is the entropy and $T$ is the temperature. In this thesis we will only deal with systems that are not electronically excited and the internal energy corresponds to the sum of the potential and the kinetic energies. In order to determine what phase that is stable at given N,T,V, the free energy of the phases should be compared. Characteristic of a first-order transition is that the free energy surface of each phase exhibits a dominant local minimum. These minima are separated by a free energy barrier as illustrated in Fig. 3.1.

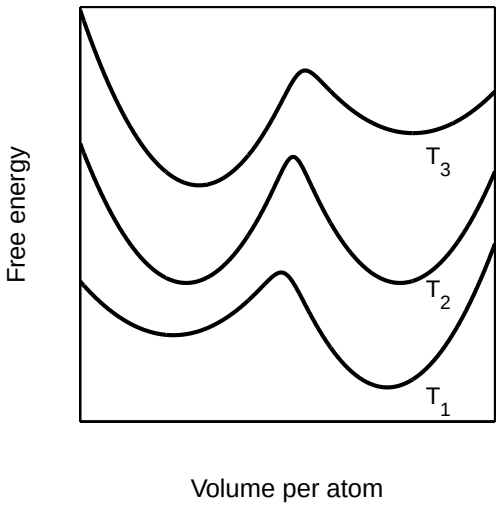


Figure 3.1: Schematic variation of the free energy for three different temperatures ($T_1 < T_2 < T_3$). At $T_2$ the transition occurs.

The phase with the lowest free energy is the equilibrium state. Say that the temperature of a system is so low that the dominant term in the free energy is the potential energy $U$. The potential energy of any liquid structure is greater than that of the solid structure and thus the system will be solid. However, with increasing temperature, the greater entropy of the liquid phase will eventually bring the system to a point where the local minima are equal. At this point the two phases coexist. Further increase of the temperature makes the liquid phase stable. The system is not static and fluctuations occur constantly. Occasionally, a fluctuation can bring the system from the stable phase to the unstable phase. In a bulk system with an almost infinite number of atoms, fluctuations to the unstable phase are however very improbable. The two phases can only coexist at a definite temperature for a given volume. In contrast, in a system with very few atoms, such fluctuations are more frequent as will be discussed in Sec. 3.3. Two phases of a finite system therefore coexist over a finite temperature range.

In a first-order phase transition, the only extensive property of the phases that is equal at coexistence is the free energy. Quantities such as for instance the internal energy per atom generally differ, also at the very melting. In a caloric curve (i.e. energy versus temperature), this is clearly demonstrated by a step in potential energy at the phase transition temperature. The same step, although rounded, can be seen for many clusters (see Fig. 5.1). This step is actually one of the most obvious indications of phase transition. A system that shows a second-order transition lacks the definite minimum of the free energy surface in configuration space. When approaching a phase transition from low temperatures, the competing minima will approach each other in configuration space. Also the potential energies of the phases approach each other and become equal at the transition temperature. A second-order

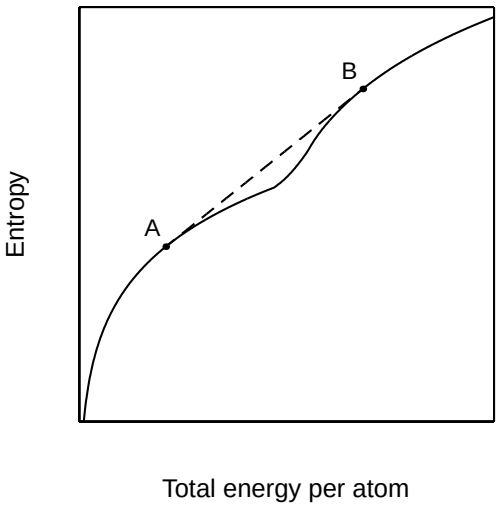


Figure 3.2: The solid curve shows the entropy as a function of the total energy per atom when a bulk system is not allowed to segregate into phases. Any convex part of the curve corresponds to instability and the dashed line describes the entropy when the system is allowed to segregate into coexisting phases. In constrast, an ensemble of clusters may follow the solid curve.

transition is therefore characterized by a kink (higher order nonanalyticity) in the potential energy, rather than a step [107]. With one exception, $Pd_{34}$,the behaviour of the palladium clusters in this work, show clearly that the melting approaches a first-order transition with increasing cluster size.

In an isolated system, for which the fixed parameters are the number of atoms $N$, the volume $V$, and the total energy $E$, a first-order phase transition occurs over a finite energy interval. The interval corresponds in the infinite system limit to a fixed temperature, i.e. the kinetic energy per atom is constant. During the melting, the increase of total energy is used to bring the system from a state of low internal energy to a high internal energy. This energy is called the latent heat. The fundamental equation of the system that totally governs the its behaviour is the entropy as a function of energy, volume and particle number,

$$S = S\left(E, V, N\right) \tag{3.1}$$

In a schematic graph of the entropy versus one of the variables, a stable phase is characterized by a concave function (Fig. 3.2). In the convex region between points A and B in Fig. 3.2 the system is unstable and will spontaneously split up in fractions of both phases. The entropy, which is an extensive quantity, will thus increase linearly when the fraction of the high-temperature phase gradually goes from zero to one. Thus, the system will instead follow the dashed line in Fig. 3.2.

## 3.2 The density of states

A concept in close connection with the entropy is the density of states $\Omega(E)$. Their relation is given by

$$S = k_B \ln \Omega, \tag{3.2}$$

where $k_B$ is Boltzmann's constant. In a quantum system, the density of states is defined as the number of states available per unit energy interval. However, when considering classical systems, a "state" is not as clearly defined. In 1875-1878, Willard Gibbs defined the partition function of a system of $n$ coordinates and $n$ momenta as [106]

$$Z = \frac{1}{h^n} \int \exp\left(-\frac{E(q_1,...,q_n,p_1,...,p_n)}{k_B T}\right) dq_1...dq_n dp_1...dp_n \tag{3.3}$$

Since then, quantum mechanics entered science and the quantum partition function is defined as a sum over all states $j$ or an integral over the density of states (DOS)

$$Z = \sum_j \exp\left(-\frac{E_j}{k_B T}\right) = \int_{-\infty}^{\infty} \Omega(E) \exp\left(-\frac{E}{k_B T}\right) dE \tag{3.4}$$

At high energies, classical and quantum mechanics should be equivalent and the partition functions according to Eqs. 3.3 and 3.4 should be equal. The classical DOS can hence be identified as

$$\Omega(E)\, dE = \frac{\int_{V(E,E+dE)} dq_1...dq_n dp_1...dp_n}{h^n} \tag{3.5}$$

where $V(E, E+dE)$ is the available phase volume for the energy interval $[E, E+dE]$. Here $h$ is Planck's constant.

## 3.3 The phase concept for finite systems

In the early interpretations of cluster simulations, conflicting statements were made about whether clusters melt with a sharp transition or with a coexistence of the phases over a finite temperature interval [48]. By coexistence we do not mean two phases in contact with each other but rather that an equilibrium ratio of number of solid to number of molten clusters is established in an ensemble of clusters [108]. It is now generally accepted that the phases coexist over a finite temperature interval. It was shown that the sharp transition between phases in a first-order transition of an infinite system arises in the limit when the number of atoms $n \to \infty$. With the assumption that a cluster can only take on two distinct states (phases) [109], the sharp transition is rounded. In this thesis the corresponding assumption will be referred to as the two-state approximation [48]. In an ensemble of clusters at

a fixed temperature, the melting/freezing can be described as a unimolecular isomerization reaction

$$\mathrm{Pd}_n\,(\mathrm{s}) \rightleftharpoons \mathrm{Pd}_n\,(\mathrm{m}) \tag{3.6}$$

In the two-state approximation, the equilibrium constant is

$$K = \frac{[\mathrm{Pd}_n\,(\mathrm{m})]}{[\mathrm{Pd}_n\,(\mathrm{s})]} = \exp\left(-\left(F_m - F_s\right)/k_B T\right). \tag{3.7}$$

where $F_m$ and $F_s$ are Helmholtz free energy for the molten and the solid cluster, respectively. For small clusters, $K$ gradually goes from zero to $\infty$ with increasing temperature. When $n$ is large, the free energy per atom, $f$, is independent of $n$ and can be written as $F = nf$. The equilibrium constant is then

$$K = \exp\left(-n\left(f_m - f_s\right)/k_b T\right). \tag{3.8}$$

When $n \longrightarrow \infty$, $K$ exhibits a singularity when $f_m - f_s$ switches sign, i.e. the phase transition is sharp. The rounding of the transition is perhaps most obvious in the caloric curve or in the graph of the heat capacity versus temperature. At the melting, the heat capacity has a peak but due to the rounding, the peak has a finite width. All my simulations (except the simulations of $\mathrm{Pd}_{34}$) confirm the two-state approximation. In Fig. 3.3, the heat capacity of $\mathrm{Pd}_{13}$, $\mathrm{Pd}_{55}$ and $\mathrm{Pd}_{147}$ are plotted. The width of the coexistence interval is finite, and the equilibrium constant is only valid if there are local minima in free energy for both phases. Berry and coworkers showed that local minima are present only within a finite temperature interval [110]. Outside this interval strictly one phase is present [110, 111]. The width of the coexistence interval, i.e. the interval where both the phases are present, can be estimated by [112]

$$\Delta T \sim \frac{T_m^2 k_B}{nA}, \tag{3.9}$$

where $A$ is the latent heat per particle and $T_m$ is the melting temperature. The melting point is often defined as the temperature where the heat capacity is maximal. Since the latent heat per particle and the melting temperature do not change dramatically with number of atoms the coexistence interval must approach zero when $n \to \infty$. The coexistence widths do shorten with cluster size in Fig. 3.3.

The difference between solid and liquid phases is often obvious for bulk systems. The atoms become mobile and the material loses its well-defined shape as the solid melts. For small clusters, the phase change is less obvious. However, in simulations some characteristics are mostly found. Upon melting, the cluster atoms become mobile, first the surface atoms and then also the core atoms. The mobility can be measured by the ratio of the timescale of vibrations to the timescale of switches between different structures of the cluster. Amar and Berry [48, 113] found for cluster that this ratio was less than 100 for molten clusters, but many orders of magnitudes larger for solid

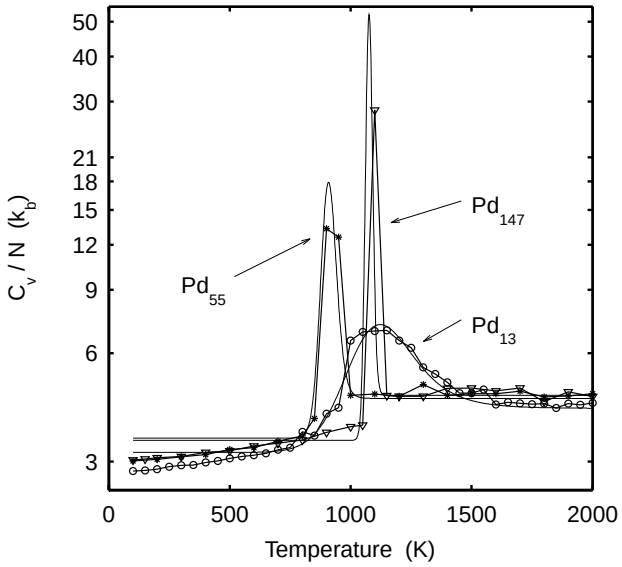


Figure 3.3: The heat capacity per atom from the MC simulations are shown at fixed $T$ of $Pd_{13}$ (rings), $Pd_{55}$ (stars) and $Pd_{147}$ (triangles). The solid lines are derived from Eq. 3.12. NB: logarithmic scale on the ordinata.

clusters. The mobility can be measured by the Lindemann index which is also called the relative bond length fluctuations [48]

$$\delta = \frac{2}{n\,(n-1)} \sum_{i=1}^{n} \sum_{j=i+1}^{n} \frac{\sqrt{\left\langle r_{ij}^2 \right\rangle_T - \langle r_{ij} \rangle_T^2}}{\langle r_{ij} \rangle_T}. \tag{3.10}$$

where $\langle r_{ij} \rangle_T$ is the average distance between atoms $i$ and $j$. $\delta$ increases at the onset of particle mobility. Thus, sampling of $\delta$ in a Monte Carlo simulation is a tool for indicating when melting starts. Lindemann's criterion for melting of bulk is that $\delta$ exceeds 10% [114]. This criterion has also been used and verified in simulations of clusters [46]. A more stringent definition of phases is to use the local minima of the potential energy surface. Each minimum can be called a catchment region, basin [115] or inherent structure [116]. The idea is that any configuration of a cluster will upon a rapid quenching fall into one of these basins. Such a basin will in this thesis be called an isomer. The isomers can now be classified as belonging to different phases, for instance according to minimum potential energy or to geometric structure. At temperatures above melting, the cluster frequently switches between different isomers and we say that the many isomers together constitute the molten phase. The number of isomers constituting the molten phase is enormous. This number is believed to increase exponentially and for $LJ_{55}$, Doye *et al.* [117] estimated the number of molten isomers to be approximately $10^{21}$. In contrast, the minimum energy isomer of the icosahedral clusters is likely to be exclusively dominant in the solid phase as mentioned above.

The entropy of a finite system as a function of the total energy can be schematically illustrated by Fig. 3.2. Very small systems cannot sustain fractions of molten and solid structure. As a consequence, the curve will be convex at the melting for a small cluster [49].

The phase transition of small metal clusters with characteristic solid and molten isomers approaches first order character with increasing $n$. Investigations of the molecular cluster $(TeF_6)_n$ indicates, however, that when $n \to \infty$, this cluster will show second order transition [118]. In these clusters, different phases of orientational order are present at different temperatures.

Surface melting has been an issue of debate [119]. The term surface melting is used for clusters which feature a premelting phase transition involving the surface atoms only. In this phase, the surface atoms might show an organized and collective motion around the core. Although we have observed that surface atoms change positions at temperatures below the melting, no real molten phase of the surface was found. Besides surface melting, the cluster may undergo solid structural transformations below the melting point. Doje and Wales found a fascinating reconstruction of the Mackay icosahedra with $n = 561$ and $n = 923$ into anti-Mackay icosahedra at a temperature well below the melting temperature [120].

## 3.4 A two-state model for the density of states

In accordance with the two-state approximation [48] that the cluster must either be entirely solid or molten, we have used a simple two-state model for the density of states of clusters with a typical coexistence melting or freezing region, as for instance the icosahedral clusters:

$$\Omega(E) = \Omega_s(E) + \Omega_m(E) \propto (E - E_0)^{n_1} + k_2 (E - E_0)^{n_2} . \qquad (3.11)$$

Here $\Omega_s(E)$ and $\Omega_m(E)$ are the DOS of the solid and molten phases, respectively, at the total energy $E$. The vibration, translation and rotation of the cluster give rise to power law terms like $(E - E_0)^{exponent}$, but to account for the anharmonicity of the vibrations, the exponents $n_1$ and $n_2$ are adjustable parameters. Although $E_0$ may be calculated by a search for the ground state configuration of a cluster, it is regarded an adjustable parameter as well. The prefactor $k_2$ is the last parameter while the prefactor of the solid phase term is arbitrarily set to unity. Note that only the relative magnitude of the solid and the molten phase contributions will be of significance in our discussion of the melting transition and cluster properties below.

The temperature-dependent caloric equation based on this model is obtained as

$$\langle E \rangle_T = \frac{\int_{E_0}^{\infty} E \cdot \Omega(E) \exp(-E/k_B T)\, dE}{\int_{E_0}^{\infty} \Omega(E) \exp(-E/k_B T)\, dE}$$

$$= E_0 + k_B T \frac{\Gamma(n_1+2) + (k_B T)^{n_2-n_1} k_2 \Gamma(n_2+2)}{\Gamma(n_1+1) + (k_B T)^{n_2-n_1} k_2 \Gamma(n_2+1)}, \quad (3.12)$$

where $\Gamma(x)$ is the gamma function. In order to calculate the caloric equation in the microcanonical ensemble (i.e. the kinetic or the potential energy as a function of the total energy) for the model DOS, an introduction of the DOS for the kinetic energy $\Omega_{kin}$ and the potential energy $\Omega_{pot}$ is necessary. The derivation of these functions is shown in **Paper I**. The caloric equation will be found to be

$$\begin{aligned} \langle E_K \rangle_E &= \int_0^{E-E_0} E_K \cdot \frac{\Omega_{kin}(E_k)\,\Omega_{pot}(E-E_k)}{\Omega(E)} dE_K \\ &= \frac{3n}{2}(E-E_0) \frac{1 + k_2 \frac{n_1+1}{n_2+1} (E-E_0)^{(n_2-n_1)}}{n_1 + 1 + k_2 (n_1+1)(E-E_0)^{(n_2-n_1)}} \end{aligned} \quad (3.13)$$

Recall that $n$ is the number of atoms of the cluster. The parameters $n_1$, $n_2$, $E_0$ and $k_2$ can be calculated by a least-square fit to the simulation results. The melting temperature in the canonical ensemble and the melting total energy in the microcanonical ensemble may now be calculated using the fitted parameters. The melting point criterion that we have used is that the equilibrium constant in Eq. 3.8 should be unity. In the canonical ensemble the corresponding criterion is that the partition functions of the two phases

$$z_s = \int_{E_0}^{\infty} \Omega_s(E) \exp(-E/k_B T)\, dE, \quad (3.14)$$

$$z_m = \int_{E_0}^{\infty} \Omega_m(E) \exp(-E/k_B T)\, dE, \quad (3.15)$$

should be equal. Using the model DOS, the expression for the melting temperature will be

$$T_M = \frac{1}{k_B} \left( k_2 \frac{\Gamma(n_2+1)}{\Gamma(n_1+1)} \right)^{1/(n_1-n_2)}. \quad (3.16)$$

With the model DOS our definition of the melting point is found to differ negligibly compared to the temperature for which the heat capacity is maximal. In the microcanonical ensemble the melting point criterion is equivalent to the condition that $\Omega_s(E_M) = \Omega_s(E_M)$. Using the model DOS the expression for the melting energy will be

$$E_M = E_0 + (k_2)^{1/(n_1-n_2)}. \quad (3.17)$$

The two-state model DOS will be used for three purposes. First, it is fitted to simulation caloric curves in the canonical ensemble (Fig. 5.1) and the accurate agreement shows that the two-state approximation is realistic.

Second, the model is fitted to microcanonical simulation caloric curves. The agreement between the fitted parameters in the canonical ensemble and the microcanonical ensemble illustrates the equivalence of the two ensembles (see Tables 1 and 2 in **Paper I**). Third, the model DOS is used to convert microcanonical data into temperature-dependent data in order to compare, for instance, the radii of gyration of the cluster in the two ensembles. In an isolated system where the total energy is conserved, the distribution of the kinetic energy is extremely narrow if the number of particles is large. Hence the temperature is well defined and the system might as well be considered to be canonical distributed [121]. In contrast, the distribution of the kinetic energy in $Pd_{13}$ is wide at fixed total energy. If an average $\langle A \rangle_E$ of the quantity $A$ is known for all total energies $E$, the average $\langle A \rangle_T$ at a certain temperature $T$ can be calculated by a weighted integration over all energies

$$\langle A \rangle_T = \frac{\int_{E_0}^{\infty} \langle A \rangle_E \, \Omega(E) \cdot \exp(-E/k_B T) \, dE}{\int_{E_0}^{\infty} \Omega(E) \cdot \exp(-E/k_B T) \, dE}. \tag{3.18}$$

As simulation data from the microcanonical simulations is available only up to a maximal energy $E_{max}$, the integrals in Eq. 3.18 must be truncated. If the temperature is not too high, the truncation error may however be negligible as the contribution is insignificant for large $E$. The conversion of energy-dependent data into temperature-dependent data is done by insertion of the model DOS.

# Chapter 4

# Simulation techniques

In this chapter we describe some simulation techniques for the calculation of average properties of systems in equilibrium. The simulation details for the energy transfer calculations will be presented in Part II.

## 4.1 Ensembles for describing the equilibrium properties of the cluster

### 4.1.1 The canonical ensemble

The properties that are to be measured or calculated for a system in equilibrium are time averages. For instance, the force that a gas chamber wall experiences changes from instant to instant and thus the pressure must be defined as the average force per wall area during a certain time. A fundamental assumption in statistical thermodynamics is that instead of taking the average of a property during an infinite time interval, the property can as well be calculated as a weighted average over the total phase space of the system. A canonical ensemble of the system is an infinite set of replicas of the system where all replicas have the same volume and the same number of atoms. The energy is however free to flow between the replicas in order to maintain a fixed temperature in all the replicas. A configuration of the system is a certain point in the phase space, $\mathbf{\Gamma}$, i.e. all the coordinates and momenta are specified. The probability that the configuration in one replica of the ensemble is $\mathbf{\Gamma}$ is given by the Boltzmann factor,

$$probability\left(\mathbf{\Gamma}\right) \propto \exp\left(-E\left(\mathbf{\Gamma}\right)/k_B T\right), \tag{4.1}$$

where $E\left(\mathbf{\Gamma}\right)$ is the total energy of the configuration. This probability distribution of the configurations is also valid in the system during infinite time.

In a closed system the number of atoms is fixed. Moreover, the common experimental situation is that the temperature also is well-defined. More complex is the matter of the volume. It is in experiments commonly rather the pressure than the volume that is an adjustable parameter. The pressure

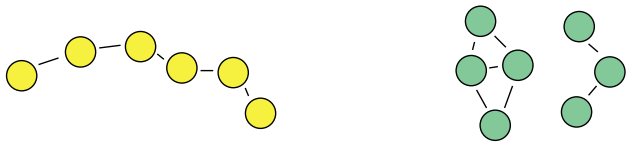

Figure 4.1: Examples of non-fragmented (left) and fragmented (right) cluster configurations according to our definition.

corresponds to a certain volume, that is true, but since the compressibility of solids and liquids is low, a small error in volume will cause a pressure which is far from the desired one. Therefore, the isobaric-isothermal ensemble with fixed number of atoms, temperature and pressure is often used for simulation of solids and liquids.

The situation is more complicated for clusters. The desire is to simulate an ensemble of a single cluster that is free to appear in any relevant geometric configuration. However, at any temperature the equilibrium state of a cluster is a total evaporation of all atoms if the cluster is not confined to a finite volume. The reason is that although the probability for the ground state configuration of the cluster might be considerably larger than for all other configurations according to the Boltzmann distribution in Eq. 4.1, the phase volume of all totally evaporated configurations is infinite. On the other hand, if the cluster is confined to a finite volume, an equilibrium will be established between evaporated atoms and the remaining cluster. The finite volume implies an undesired non-zero pressure and the number of atoms of the cluster may be difficult to define.

A common way to simulate a cluster is to reject all configurations that are considered to represent a fragmented cluster. One way is to confine the cluster to a small sphere [47, 122]. However, there is a risk that spherical shapes of the cluster are favoured. As will be seen, the small clusters are not at all spherical in the molten phase. Cheng *et al.* [50] proposed the simulation of clusters at constant pressure and the evaluation of the volume from the relation

$$V = -\left(\frac{\partial G}{\partial P}\right)_T \tag{4.2}$$

where $G$ is Gibbs free energy and $P$ is the pressure. Our definition of a non-fragmented cluster is that it should be possible to make a chain of bonds from any cluster atom to any other. With this definition, the atoms to the left in Fig. 4.1. describe a cluster in contrast to the atoms to the right. The advantage of this definition is that spherical shapes of the cluster are not favoured.

Here a bond is only an indication of a short interatomic distance. Two atoms are supposed to be bonded if they are closer to each other than a distance $B$. The exact choice of $B$ is not crucial and any $B$ between 4 and 5.8 Å resulted in the same distinction between fragmented and non-fragmented

clusters for the potential parameters that we have used. Furthermore, the vapour pressure of palladium is so low that rapid evaporation occurs only many hundred kelvin above the melting point [115].

### 4.1.2 The isobaric-isothermal ensemble

In the isobaric-isothermal ensembles the number of atoms, the pressure and the temperature are constant and the volume is treated as a variable equivalent to the coordinates and the momenta of the atoms. When the volume is changed, the atomic coordinates are correspondingly scaled so that the "similar" system is obtained. The probability for a configuration with a certain volume is [123]

$$probability\left(\mathbf{\Gamma}, V\right) \propto \exp\left(-\left(E\left(\mathbf{\Gamma}, V\right) - PV\right)/k_B T + n \ln V\right), \tag{4.3}$$

where $E\left(\mathbf{\Gamma}, V\right)$ is the total energy of the configuration. In Sec. 5.3 we refer to our unpublished work on simulations of bulk palladium where this NPT-ensemble was used.

### 4.1.3 The microcanonical ensemble

In the microcanonical ensemble, the fixed temperature is replaced by a fixed total energy. Since a single isolated cluster forms a constant-energy system, this ensemble is of relevance for the study of the properties of a cluster without the thermal averaging that the Boltzmann distribution implies. In the simulations we are only interested in features regarding the spatial configuration and thus we would like to simulate the cluster coordinates only, disregarding the momenta. Although the spatial configurations and momenta are connected via the total energy conservation, it is possible to sample the spatial configurations only. For the sampling of quantities we have used the Efficient Microcanonical Sampling (EMS) method developed by Severin *et al.* [124]. A detailed description of this method is also found in Ref. [125]. In the microcanonical system, all states are equally probable. Therefore, the probability of a spatial configuration $\mathbf{R}$ must be proportional to the number of momentum states available when the kinetic energy is $E_K = E - U\left(\mathbf{R}\right)$. The number of momentum states is proportional to the density of momentum states,

$$\Omega_K\left(E_K\right) = constant \cdot E_K^{3n/2-1}. \tag{4.4}$$

and the probability for a spatial configuration is given by

$$probability\left(\mathbf{R}\right) \propto \left(E - U\left(\mathbf{R}\right)\right)^{3n/2-1}. \tag{4.5}$$

The microcanonical ensemble may now be simulated exactly like the canonical ensemble, only replacing Eq. 4.1 by Eq. 4.5.

## 4.2 Simulation methods

### 4.2.1 Molecular dynamics simulation

There are two dominant methods for simulation of atomic systems, molecular dynamics (MD) and Monte Carlo (MC) simulation. Among these two, the MD simulation is the most intuitive method with the great advantage that the time-development of the system can be followed within a well defined time-scale. In MD simulation, the newtonian equation of motion is solved for all atoms in the system. MD is the natural choice when the dynamics of the system is of importance. Hence, the cluster collisions will be simulated by means of MD simulation.

The newtonian mechanics is based on energy conservation, i.e. the system is microcanonical. In order to use MD simulation in the canonical ensemble, thermostat techniques have been developed [123]. The melting simulations that are to be presented below have been compared with simulations by Grönbeck *et al.* [34] in which the MD technique with the Nosé-Hoover thermostat [35] was used.

### 4.2.2 Metropolis Monte Carlo simulation

In 1953, Metropolis *et al.* [126] presented a new simulation technique that today is a standard for calculation of thermodynamical averages. Say that in a given ensemble, the probability for a configuration is given by

$$probability\left(\mathbf{\Gamma}\right) \propto f\left(\mathbf{\Gamma}\right). \tag{4.6}$$

The average of the quantity $A\left(\mathbf{\Gamma}\right)$ is then simply

$$\left\langle A\right\rangle = \frac{\int A\left(\mathbf{\Gamma}\right) f\left(\mathbf{\Gamma}\right) d\mathbf{\Gamma}}{\int f\left(\mathbf{\Gamma}\right) d\mathbf{\Gamma}} \tag{4.7}$$

Often, both $A\left(\mathbf{\Gamma}\right)$ and $f\left(\mathbf{\Gamma}\right)$ are analytical expressions but the dimensionality of the integrals is so high that a numerical integration is impossible. An alternative calculation would be to randomly generate configurations $\mathbf{\Gamma}_i$ and calculate the average

$$\left\langle A\right\rangle = \frac{\sum_i A\left(\mathbf{\Gamma}_i\right) f\left(\mathbf{\Gamma}_i\right)}{\sum_i f\left(\mathbf{\Gamma}_i\right)} \tag{4.8}$$

Unfortunately, the distribution function $f\left(\mathbf{\Gamma}\right)$ is often a very nonsmooth function in thermodynamical systems and $f\left(\mathbf{\Gamma}\right)$ is significant only for a very small fraction of all configurations. The contribution of Metropolis was to develop a scheme to generate configurations according to $f\left(\mathbf{\Gamma}\right)$. The generated configurations will thus mostly be the ones that the system is likely to occupy. This is called importance sampling. The average is then simply

$$\left\langle A\right\rangle = \frac{1}{n}\sum_{i=1}^{n} A\left(\mathbf{\Gamma}_i\right). \tag{4.9}$$

In practise, a simulation is started with the system in a configuration that is representative of equilibrium. A new trial configuration is generated by a small random change of the present configuration. The probabilities of the present and the trial configurations are compared. If the ratio $f(\mathbf{\Gamma}_{trail})/f(\mathbf{\Gamma}_{present})$ is larger than a uniformly distributed random number between zero and one, the trial configuration is accepted as the next configuration in Eq. 4.9. Otherwise the next configuration will be identical with the present one. This procedure is iterated so that $N$ configurations are generated. By some user-defined criterion it must now be checked that $\langle A \rangle$ has converged sufficiently to the correct value. The presence of barriers between different parts of the phase space may however severely prevent an ergodic exploration of the phase space and the converged average $\langle A \rangle$ may not be correct. For a more detailed description of the MC and MD techniques, see Ref. [123].

In this work MC simulations have been carried out in the canonical and microcanonical ensembles. New configurations are generated by changing the position of a randomly picked atom by a small displacement. The displacement is adjusted to give approximately 50% rejection. In the further discussion we will refer to MC "steps" and "macro steps". One step is the trial displacement of one atom. In a system with $n$ atoms, a macro step is equal to $n$ steps.

The great advantage of the MC technique is in my opinion that model systems can easily be studied, since no restrictions are placed on the probability distribution $f(\mathbf{\Gamma})$. For instance, the potential energy need not be differentiable. Non-differentiable potentials are however a complication in MD simulations.

### 4.2.3 The Reference System Equilibration method

The Reference System Equilibration method (RSE) was developed by Ming, Nordholm and Schranz [127] and has to our knowledge only been employed for test cases. But, as will be shown, the RSE is an excellent method by which to obtain the anharmonic density of states for realistic systems. The DOS is obtained by a simulation of the system (the cluster) and an appropriate reference system such that the cluster can exchange energy with the reference system. There is however no interaction between the two systems. In our simulations the reference system consists of $n_H$ three-dimensional harmonic oscillators but the reference system might be any system with a known DOS.

A combined system is created by fusing a cluster of $n$ atoms and $n_H$ three-dimensional harmonic oscillators. Due to energy exchange, the potential and kinetic energies of the cluster and the oscillators, respectively, will fluctuate resulting in distributions of potential energy of the cluster and of the harmonic oscillators. The distribution of energy is determined by the DOS of the cluster and the oscillators and this is the basic fact used in the RSE.

A state of the combined system is defined by all configurations and momenta of all cluster atoms and harmonic oscillators. Since all states in this combined microcanonical system are equally probable, the probability distribution for the cluster to have total energy $E_C$ is given by

$$f\left(E_C\right) = \frac{1}{\Omega_{CH}\left(E_{CH}\right)} \Omega_C\left(E_C\right) \Omega_H\left(E_{CH} - E_C\right) \tag{4.10}$$

Here $E_C$ is the total energy of the cluster and $\Omega_C\left(E_C\right)$ and $\Omega_H\left(E_H\right)$ are the DOS of the cluster and the reference system, respectively. The inverse of the DOS of the combined system at the total energy $E_{CH}$ is $\Omega_{CH}^{-1}\left(E_{CH}\right)$, which works as a normalization constant when $E_{CH}$ is fixed. As will be shown below, the normalization constant is only known in very special cases. The DOS of one harmonic oscillator is analytically known and by convolution, the DOS of the reference system is obtained as

$$\Omega_H\left(E_H\right) = \frac{1}{h^{3n_H}\,\Gamma\left(3n_H\right)} \left(\frac{2m}{C}\right)^{3n_H/2} E_H^{3n_H-1}. \tag{4.11}$$

where $h$ is Planck's constant, $E_H$ is the total energy of the reference system, $m$ is the mass of an oscillator and $2C$ is the force constant of the restoring force of one oscillator. Note that in the RSE context $\Gamma$ denotes the gamma function.

A combined spatial configuration $\mathbf{R}_{CH} = [\mathbf{R}_C, \mathbf{R}_H]$ is a vector of all $n+n_H$ spatial coordinates. The potential energy is $U_{CH}\left(\mathbf{R}_{CH}\right) = U_C\left(\mathbf{R}_C\right) + U_H\left(\mathbf{R}_H\right)$. The probability for such a configuration is proportional to the number of momentum states for the remaining kinetic energy.

$$f\left(\mathbf{R}_{CH}\right) \propto \Omega_{CH,kinetic}\left(E_{CH,kinetic}\right) \propto \left(E_{CH} - U_C - U_H\right)^{(3n+3n_H)/2-1}. \tag{4.12}$$

Although the spatial configuration is specified, kinetic energy might flow between the cluster and the reference system. Hence, the total energy of the cluster fluctuates and is distributed according to

$$\begin{aligned} f\left(E_C\,|\mathbf{R}_{CH}\right) &= B \cdot \Omega_{C,kinetic}\left(E_C - U_C\right) \cdot \Omega_{H,kinetic}\left(E_{CH} - E_C - U_H\right) \\ &= B' \cdot \left(E_C - U_C\right)^{3n/2-1} \cdot \left(E_{CH} - E_C - U_H\right)^{3n_H/2-1}, \end{aligned} \tag{4.13}$$

where

$$B' = \frac{\Gamma\left(3\left(n+n_H\right)/2\right)}{\Gamma\left(3n/2\right)\Gamma\left(3n_H/2\right)} \cdot \frac{1}{\left(E_{CH} - U_C - U_H\right)^{3(n+n_H)/2-1}}. \tag{4.14}$$

By a microcanonical sampling, $\mathbf{R}_{CH}$ will be distributed correctly in the phase space and the distribution of the total cluster energy at fixed total energy of the combined system is

$$\begin{aligned} f\left(E_C\right) &= \left\langle f\left(E_C\,|\mathbf{R}_{CH}\right)\right\rangle = \\ &\left\langle \frac{\Gamma\left(3\left(n+n_H\right)/2\right)}{\Gamma\left(3n/2\right)\Gamma\left(3n_H/2\right)} \cdot \frac{\left(E_C - U_C\right)^{3n/2-1} \cdot \left(E_{CH} - E_C - U_H\right)^{3n_H/2-1}}{\left(E_{CH} - U_C - U_H\right)^{3(n+n_H)/2-1}} \right\rangle. \end{aligned} \tag{4.15}$$

Apart from the prefactor $\Omega_{CH}(E_{CH})$, the DOS of the cluster can be calculated using Eqs. 4.10 and 4.15:

$$\Omega_C(E_C) = \Omega_{CH}(E_{CH}) \frac{f(E_C)}{\Omega_H(E_{CH} - E_C)} \tag{4.16}$$

The numerical accuracy is acceptable only in a short interval of $E_C$. In order to obtain high accuracy of the DOS in the whole range from the minimal energy $E_0$ to above melting, a number of simulations with increasing $E_{CH}$ must be run. With the condition that the DOS should be continuous the overlapping of intervals of accurate representation can form the whole DOS.

By overlapping of intervals of accurate representation the total DOS is obtained apart from the prefactor. When the DOS for different isomers is to be compared this prefactor must be known. For the clusters the DOS is analytically known when the energy is so low that the atoms vibrate harmonically. In the low-energy limit, the DOS is then

$$\Omega_C(E_C) = \left(\frac{2\pi}{h}\right)^{3n-6} \frac{1}{\prod_i^{3n-6} \omega_i} \cdot \frac{\pi/4}{\Gamma(3n-3)} \cdot \frac{2\pi V}{h^3} (2nm)^{3/2} \cdot \frac{16\pi^3}{h^3} (I_a I_b I_c)^{1/2} \cdot (E_C - E_0)^{3n-4} . \tag{4.17}$$

The ingredients are the normal mode angular frequencies $\omega_i$, the volume $V$, the product of the moments of inertia along the principle axes, $I_a I_b I_c$, and the minimal potential energy of the isomer $E_0$. These properties can be calculated for a given structure and the volume which the cluster is in can be disregarded as it is equal for all isomers. Since the right-hand sides of Eqs. 4.16 and 4.17 should be equal when the energy is low, the prefactor $\Omega_{CH}(E_{CH})$ can be identified. The scheme is now complete with respect to the calculation of the absolute DOS for an isomer. In Fig. 4.2, the base-ten logarithm of the DOS of $Pd_{13}$ is drawn. Knowing the DOS, the heat capacity can be calculated and compared with the results from the canonical simulations (Fig. 4.3). The agreement shows that the DOS is correctly and accurately determined by the RSE. The dashed curve is the heat capacity according to the model DOS. The curves disagree for low temperatures. The reason is that the model DOS forces the heat capacity to be constant for low and high temperatures. In reality, the increasing anharmonicity of the solid cluster causes the heat capacity to be increasing. The melting of $Pd_{13}$ occurs around $E_C = -30.2$ eV. At this energy a convex part of $\ln\Omega$ in Fig. 4.2 can be perceived as mentioned in Sec. 3.3.

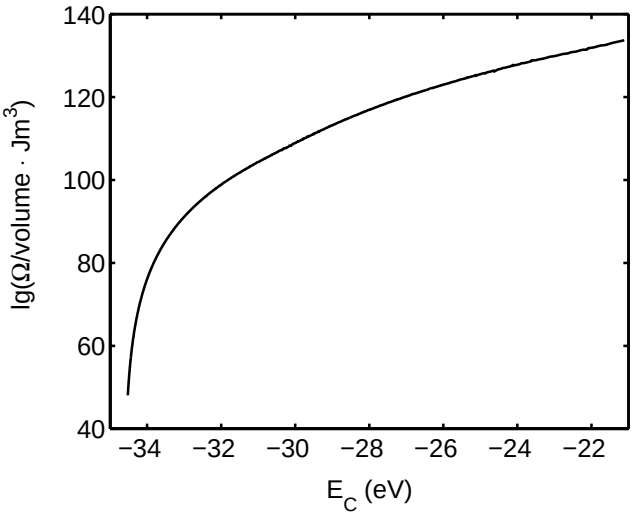


Figure 4.2: The base ten logarithm of the absolute DOS for $Pd_{13}$ divided by the volume is shown.

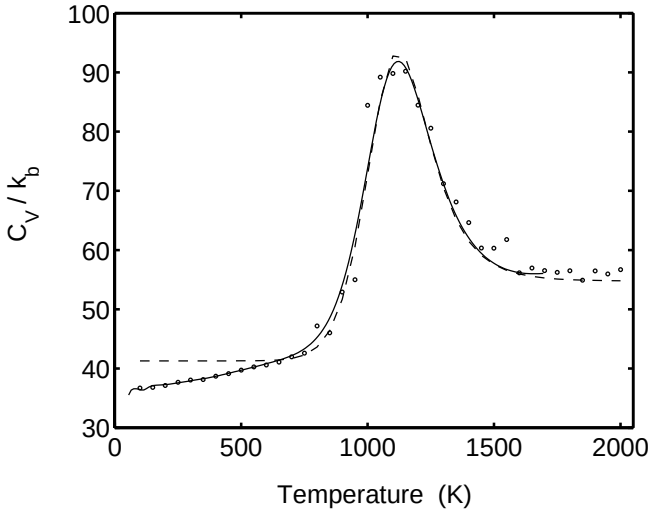


Figure 4.3: The heat capacity of $Pd_{13}$ is shown. The rings are from canonical simulations, the solid line from RSE simulations and the dashed line according to the model DOS.

# Chapter 5

# Thermal properties of the palladium clusters

In the investigation of the thermal properties of the palladium clusters, the focus has been three-fold. i) To investigate the evolution of properties like the potential energy and radii of gyration with increasing temperature or total energy. ii) To compare different ensembles and simulation techniques to find agreement and differences, advantages and disadvantages. iii) To contribute to the development of solutions to the problem with phase barriers in computer simulation.

In this work, Monte Carlo simulations with the cluster in the canonical and microcanonical ensembles, respectively, have been used. The results will be compared to simulations by Henrik Grönbeck and co-workers [34], who employed the Nosé-Hoover (fixed temperature) molecular dynamics technique. For the Monte Carlo simulations the program package MonteLab [128] was used.

## 5.1 Evolution of properties with temperature or total energy

### 5.1.1 Potential and kinetic energy

The average total energy versus temperature from the simulations at constant temperature is given in Fig. 5.1 for the icosahedral clusters $Pd_{13}$, $Pd_{55}$ and $Pd_{147}$. The solid lines display the caloric curves according to the model DOS which are calculated using Eq. 3.12 and the optimal parameters in Table 1 in **Paper I**. The rounded transition from solid to molten phase and the accurate agreement between data and the prediction of the model DOS supports the two-state picture. It is obvious from the curves that the melting interval becomes more narrow with increasing cluster size. The melting intervals can also be seen in Fig. 3.3. The heat capacity in Fig. 3.3 corresponds to the total energy in Fig. 5.1. The peak covers about 400 K for $Pd_{13}$

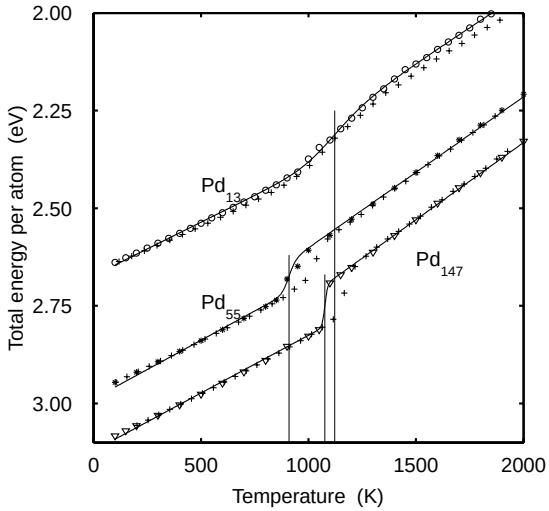


Figure 5.1: The graph shows the total energy per atom for $Pd_{13}$ (rings), $Pd_{55}$ (stars) and $Pd_{147}$ (triangles) versus $T$ according to the constant-temperature simulations. The plusses represent the outcome from the MD simulations with the Nosé-Hoover thermostat [34]. The solid lines are the caloric curves given by Eq. 3.12. The parameters of the model DOS are adjusted to fit the simulation caloric curve. The vertical lines indicate the melting points given by Eq. 3.16.

but only about 100 K for $Pd_{147}$. The thin solid heat capacity curves show the prediction of the model DOS. Also for the heat capacity the agreement is good. The vertical lines in Fig. 5.1 indicate the melting temperatures calculated by Eq. 3.16 as listed in Table 1 in **Paper I**.. Surprisingly, $Pd_{13}$ melts at the highest temperature. With the simple assumption that the melting is determined by the average coordination number in the cluster, the melting temperature should gradually increase with increasing size [129] with the bulk melting point as a limit. It has been observed that small clusters do not act according to simple scaling laws [12, 130], but that $Pd_{13}$ should melt at a higher temperature than the equally symmetric $Pd_{147}$ was not expected. However, small clusters with extreme melting temperatures has been observed in experiments [12].

The plusses in Fig. 5.1, represent the results from Grönbecks MD simulations with the Nosé-Hoover thermostat [34]. For low and high temperatures, the agreement with the MC simulations is good. However, for $Pd_{55}$ and $Pd_{147}$, the MD-NH simulations suggest a higher melting temperature. The reason for the discrepancy is not a fundamental difference in simulation technique. The reason is that in the coexistence region the recurring phase switches that should generate a correct ratio of the solid to molten phase, are obstructed by phase barriers. The MD-NH simulations were simply not sufficiently long and the solid phase was favoured.

The average potential energy minus $E_0$ and the average kinetic energy as a

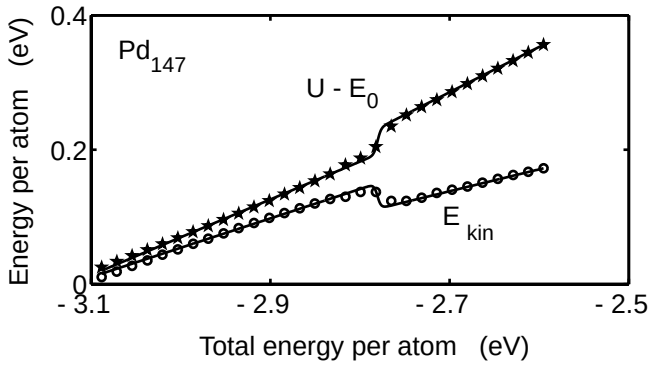


Figure 5.2: The caloric curves from simulations at fixed total energy.

function of the total energy are calculated in microcanonical MC simulations and the results for $Pd_{147}$ are displayed in Fig. 5.2. The pentagrams and the rings show simulation data and the solid curves are calculated using Eq. 3.13. Before melting, the potential energy is seen to gain more than half the available energy. The reason is that the vibrations in the cluster turn more and more anharmonic which leads to a higher heat capacity for the potential energy than the kinetic energy. At melting the curves exhibit the S-bend that is typical for two-state systems [117]. In bulk material the sign of melting is that the kinetic energy is constant while the total energy increases. During the melting, all added energy is put into the high-energy liquid structure. In contrast a two-state system cannot melt gradually and thus the cluster abruptly changes to the high-energy molten phase. The energy must be taken from the kinetic energy and a consequent drop occurs. The caloric curve in the microcanonical ensemble more obviously indicates a two-state system than does the caloric curve in the canonical ensemble.

The optimal parameters in Table 1 in **Paper I** show accurate agreement for the two ensembles, except in the case of $Pd_{147}$. The reason for the discrepancy is again the phase barrier as will be discussed later. This discrepancy will also be seen for $Pd_{147}$ in Fig. 5.3. In this figure, the converted microcanonical potential energy is drawn versus temperature together with the canonical data showing the equivalence between the ensembles.

### 5.1.2 Geometric properties and mobility

The geometry of clusters is reported to change with temperature. For some clusters, a structural change has been observed before melting as when large 561-atom clusters change from a true Mackay icosahedron to an anti-Mackay icosahedron [120]. The interaction between the atoms in the clusters was modeled by the Morse potential. In our simulations no pre-melting structural changes have been observed. Upon melting the atoms become mobile and they constantly change positions and neighbours, especially the surface

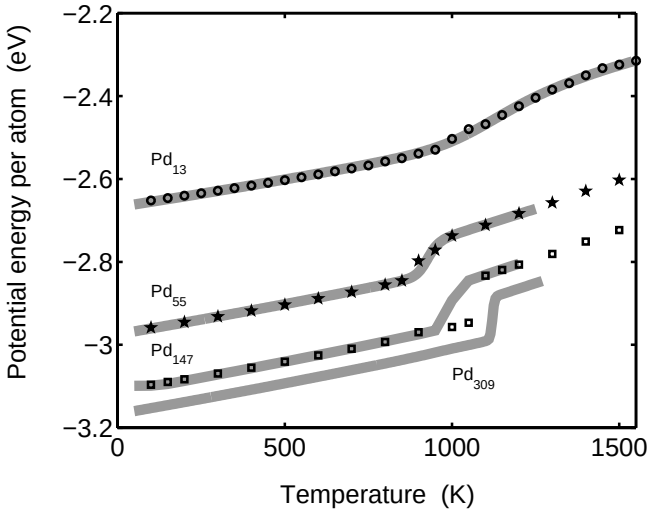


Figure 5.3: The potential energy versus temperature is shown. The solid lines show the converted microcanonical data. The lines are from the bottom: $Pd_{309}$, $Pd_{147}$, $Pd_{55}$ and $Pd_{13}$. Data from simulations at fixed temperature are shown as rings ($Pd_{13}$), pentagrams ($Pd_{55}$) and squares ($Pd_{147}$).

atoms, but also the core atoms. The fluctuations result in a split in the radii of gyration. The radii of gyration along the principle axes are defined as

$$r_i = \sqrt{\frac{I_i}{m}}, \qquad i = 1, 2, 3, \tag{5.1}$$

where $I_i$ is the moment of inertia along the principle axis $i$, and $m$ is the cluster mass. For the solid icosahedral clusters the radii of gyration are equal which can be seen in Fig. 5.4 for $Pd_{55}$. At melting, however, the radii split up and one radius of gyration is even decreasing. The same thing happens for all the icosahedral clusters but the ratio of the maximal radius to the minimal radius approaches unity with increasing cluster size. This is in accord with the general knowledge that liquid droplets assume a spherical shape to minimize the surface tension [131]. The vertical line shows the melting point in Table 1 in **Paper I**. Since the change in radii of gyration occurs at the same temperature, it is verified that the phase change is indeed a structural change.

The thick grey lines in Fig. 5.4 show the converted microcanonical results which are in good agreement with canonical results. The results from the MD simulations with Nosé-Hoover thermostat are drawn as rings [34]. The curves are in agreement with the Monte Carlo results except at the very melting. The reason for the discrepancy is the same as for the potential energy: the MD-NH simulations favoured the solid phase due to too short time-development.

Another characteristic of the geometry is the radius of the cluster. We

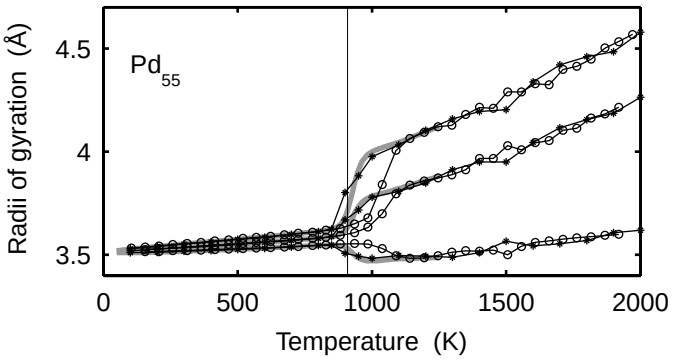


Figure 5.4: The maximal, medium and minimal radii of gyration are shown versus $T$ for $Pd_{55}$. The star-lines show the results from the fixed-temperature simulations. The thick grey lines are the converted results from the fixed-energy simulations. The vertical line indicates the melting point. The curves with rings are from the MD simulations with Nosé-Hoover thermostat in Ref. [34].

have used the mean distance to the centre of mass,

$$d_{CM} = \frac{1}{n} \sum_{i=1}^{n} |\mathbf{x}_i - \mathbf{x}_{CM}| \,, \tag{5.2}$$

as a measure of the size. Here $\mathbf{x}_i$ is the position of atom $i$ and the centre of mass is $\mathbf{x}_{CM}$. In Fig. 5.5, $d_{CM}$ for $Pd_{55}$ is shown as a star-line (canonical simulations) and thick grey line (converted from microcanonical simulation). The curves exhibit two regions of linear increase of $d_{CM}$ which correspond to the isobaric thermal expansivity of bulk material (see Fig. 5.10) [101, 107]. At the very melting the structure is made more loose, as expected. On the cover of this thesis two snapshots of $Pd_{147}$ show the cluster in the solid (left) and the molten (right) phase. Clearly the shape is considerably modified with a more spherical shape of the solid phase.

The mobility of the atoms in the cluster can be measured by the Lindemann index and in our simulations we have observed a rapid increase from approximately 0.05 to 0.3 at melting. Of importance is that $\delta$ starts the steep rise at slightly lower temperatures than the previously described quantities. The reason for this is the presence of so-called floaters [119]. Floaters are surface atoms that leave the surface to become mobile on the surface for a short time before they fall down again. Although the structure, and hence the phase, is still solid, atoms will switch positions causing $\delta$ to increase dramatically. The Lindemann index is a measure of fluctuations and the accuracy obtained in the simulations is worse than for averages. Consequently, $\delta$ is the only quantity such that the conversion from microcanonical into canonical results does not yield full equivalence as seen in Fig. 5.6.

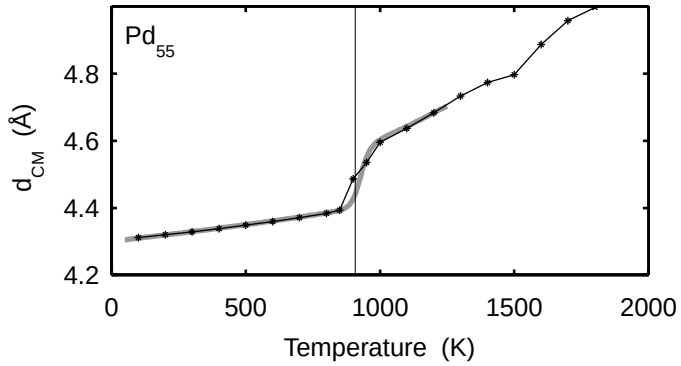


Figure 5.5: The average distance to the centre of mass, $d_{CM}$, versus $T$ for $Pd_{55}$. The vertical line indicates the melting point.

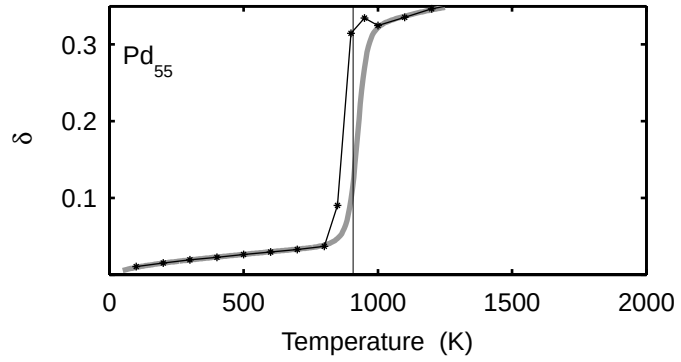


Figure 5.6: The Lindemann index $\delta$ is shown versus $T$ for $Pd_{55}$. The star-lines show the results from the fixed-temperature simulations. The thick grey lines are the converted results from the fixed-energy simulations. The vertical line indicates the melting point.

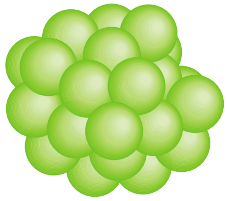

Figure 5.7: The configuration of $Pd_{34}$ with minimal potential energy found in our annealing simulations is shown.

### 5.1.3 The non-icosahedral cluster $Pd_{34}$

The icosahedral clusters that we have presented so far all fit the model of coexistence between two distinct and non-mixable states. As an example of a cluster with a different behaviour, $Pd_{34}$ is presented here. This cluster does not have a unique solid minimum-energy structure as the icosahedral clusters probably do [105]. In contrast, in a MC simulation with annealing temperature we found a couple of isomers with similar energy. The configuration with the lowest energy that we have found is depicted in Fig. 5.7. The thermal evolution of the radii of gyration, the Lindemann index and the heat capacity are shown in Fig. 5.8. The typical signs of a "first-order phase change" are missing. There is no peak in heat capacity and the radii of gyration do not exhibit a dramatic change at any temperature. The solid structure is rather to be called a glassy state, since the cluster is frozen in a highly asymmetric state. The only difference between the solid and molten phases is that the mobility of the atoms is low at low $T$, but suddenly rises at approximately 350 K. This kind of thermal behaviour has been observed for, e.g., Al clusters [132].

## 5.2 Phase barriers

Simulations are in most cases based on the ergodic principle [123], i.e., that from the initial configuration all other states can be reached within a finite number of steps. It is a well known fact that the free energy barrier between two phases may prevent a phase change on the time-scale of a simulation, although the phase change should eventually occur [123, 133, 134, 135, 136, 137]. The phase barrier causes "broken ergodicity" or "quasi-ergodicity".

### 5.2.1 Bulk melting in simulations

Let us first study the problem in simulations of bulk systems. Using periodic boundary constraints and the isothermal-isobaric ensemble [123], the melting temperature of a compound may be found by observing at what temperature the volume per particle abruptly rises. However, starting with the system in the solid phase, it may take such a long time for the system to transform into

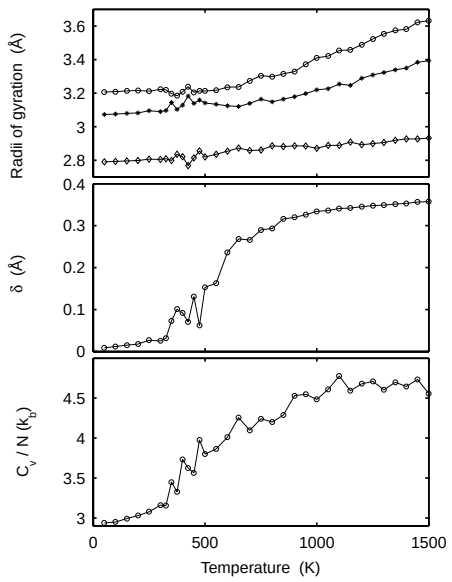


Figure 5.8: Results are shown for $Pd_{34}$ versus $T$. From above: the maximal, medium and minimal radius of gyration, $\delta$ and the heat capacity per atom.

the liquid phase that no transformation can be found in the course of a simulation, even at temperatures above the melting point [135, 136]. Belonoshko and coworkers found that the melting temperature might be overestimated by several hundred kelvin due to the phase barrier [135]. A solution to the problem is also proposed. In so-called two-phase simulations the simulation box of active atoms is split into two parts [135, 136]. Initially, the atoms in one part are arranged according to the solid phase and the other part is from a truly liquid phase. With this method both phases are present and it is supposed that at the interface, the stable phase will grow at the expense of the other phase.

In unpublished simulations we have studied bulk palladium described by the identical MBA potential and parameters using the two-phase method as well as the one-phase (only solid phase present originally) method. The initial active box of palladium atoms is depicted in Fig. 5.9. The simulation results show significant differences (see Fig. 5.10). In the one-phase simulations the initial configuration is the solid structure and the melting does not occur until 2000 K. With the two-phase method, the simulations at 1700 K or higher temperatures go from two-phase to liquid phase structure, but at 1500 K the system freezes. The results show the same behaviour as in the work of Belonoshko and coworkers [135]. The experimental curve is taken from the tables in Ref. [101].

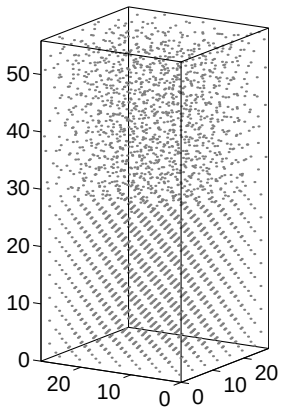


Figure 5.9: The initial configuration of two-phase simulations of palladium bulk is shown.

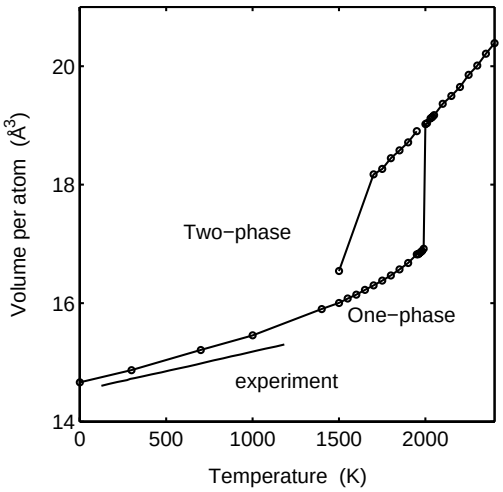


Figure 5.10: The graph shows the volume per atom of palladium bulk in isobaric-isothermal simulations at zero pressure. Both two-phase and one-phase simulations are shown. The experimental values are included as a reference.

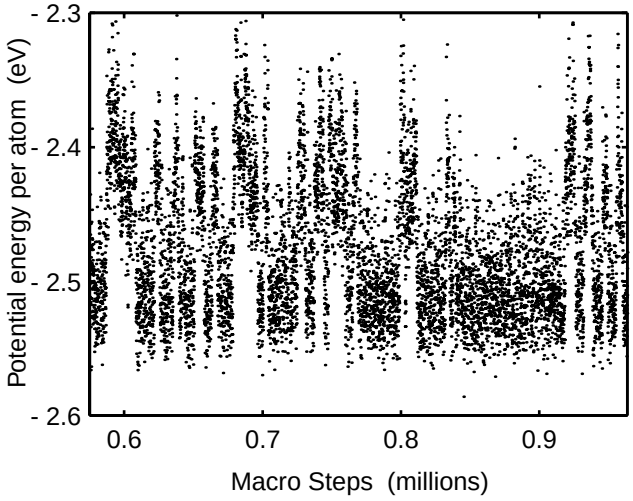


Figure 5.11: The graph shows the potential energy of $Pd_{13}$ in the course of a simulation at 1100 K. Each dot is an average over 1000 simulation steps.

### 5.2.2 Phase switches in small clusters

The situation is different for the small clusters. At temperatures in the coexistence interval, theory predicts the cluster to constantly switch between the phases. That was indeed observed for $Pd_{13}$ at 1100 K (see Fig. 5.11). The total number of steps that the cluster spends in the solid and molten phases, respectively, determines the equilibrium constant. Thus it is important to have many switches during a simulation in order to be confident that ergodic sampling is achieved.

In contrast, in the course of a simulation of $Pd_{55}$ for a reasonable time, very few phase changes occur at 900 K (see Fig. 5.12). If this simulation had been interrupted after 400 000 macro steps, which would not have been a remarkably short simulation, the cluster would have behaved as solid throughout the simulation. When a phase change occurs it is completed rapidly. With the few phase changes seen for $Pd_{55}$, an accurate determination of the equilibrium constant at this temperature is impossible. This is the reason why phase barriers make the melting temperature determination inaccurate. Furthermore, the randomness of the precise times when the phase changes occur is the reason why the melting temperature calculations of $Pd_{147}$ based on the canonical and microcanonical simulations yield different results. In the microcanonical simulations a phase change from solid to liquid happened to occur at a lower energy.

When the number of atoms increases, the melting interval shortens [112]. Thus, already at fairly small sizes the potential energy step at the melting temperature will look like at bulk melting, even if it is not. In contrast, in the microcanonical caloric curve a two-state system, regardless of size, can always be distinguished from bulk. In Fig. 5.13, the microcanonical caloric

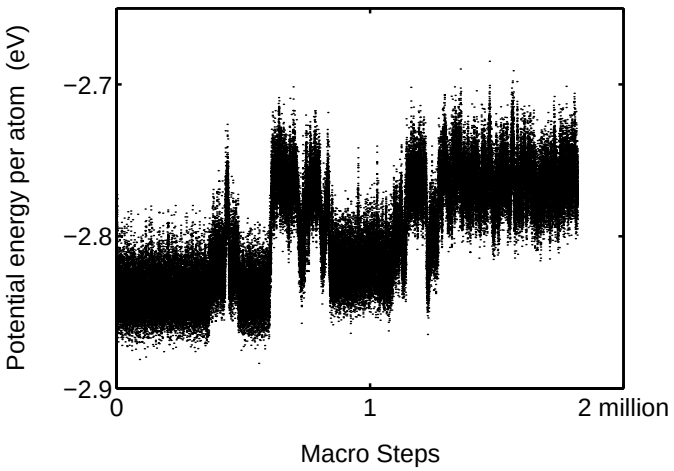


Figure 5.12: The graph shows the potential energy of $Pd_{55}$ in the course of a simulation at 900 K. Each dot is an average over 1000 simulation steps.

curve of $Pd_{309}$ is drawn.

The caloric curves show an S-bend at melting that is typical of a two-state system. However, this might be largely an artifact due to the phase barrier. Let us assume that $Pd_{309}$ is so big that it can hold both solid and molten fractions simultaneously. (That has been observed in simulations of for instance $Au_{459}$ [138].) We might then expect that the proper caloric curve should follow the grey line. However, due to the phase barrier the cluster is in intact solid phase until a total energy is reached where it should be entirely molten. Such a situation could not be distinguished from that pertaining to a two-state cluster. Conclusion: due to phase barrier, a caloric curve like the one in Fig. 5.13, is not a proof of a two-state system. Instead, a criterion to prove a two-state system is to find frequent phase switches in a simulation in the coexistence region.

### 5.2.3 Free energy barrier character

Let us go back to the curve showing the potential energy versus number of macro steps for $Pd_{55}$ at 900 K (Fig. 5.12). The phase barrier is generally to be found in the dimension of free energy [106]. In the canonical ensemble, the free energy consists of a potential energy part and an entropic part. What is the character of the phase barrier for the cluster? In Fig. 5.12, the cluster is initially in the solid phase but it melts after about 400 000 macro steps. The melting involves a step upwards in potential energy. Thus the melting is prevented by this increase in potential energy. An entropic barrier may be present as well. In contrast, when the cluster switches from molten to solid phase, there is no barrier in potential energy, only a direct step downwards. The potential energy does not obstruct the solidification at all. Still, this phase change is rare on the time-scale of a simulation due to a free energy

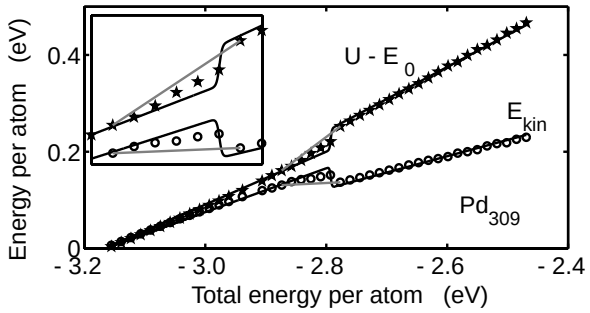


Figure 5.13: The graph shows the caloric curves of the constant-energy simulations for $Pd_{309}$. The rings show the kinetic energy and the pentagrams show the potential energy minus $E_0$ versus total energy. The solid lines are the caloric curves predicted by the model DOS. Grey lines show the caloric curves if the cluster melts in a bulk-like manner. The inset shows a magnified part of the figure.

barrier. Since the potential energy takes no part in the barrier, it must be of entropic character only.

What is an entropic phase barrier? Phase space regions might be separated by a bottleneck which is not high in potential energy but narrow. By narrow we mean that a system must take a specific path through a bottleneck to go from one part of the phase space to another. Such a bottleneck might be associated with a low entropy which implies a high free energy [139].

## 5.3 Simulation of separated phases using the Reference Equilibration Method

For each of the clusters $Pd_{55}$ and $Pd_{147}$ the DOS of the phases are to be compared. In order to do that the DOS for the solid cluster must be calculated for energies where it is superheated. For the molten cluster the situation is even more difficult, since the cluster must be supercooled all the way down to the low-energy limit where the vibrations are harmonic. Another difference between the phases is that the solid phase consists of one dominant isomer [105], but a huge number of isomers contribute to the molten phase. Doye and Wales extrapolated the number of molten isomers to approximately $10^{21}$ in a Lennard-Jones cluster with 55 atoms [117]. The DOS of all of theses isomers cannot be calculated. Instead, only one isomer has been chosen to represent the whole molten phase. This isomer has been generated from simulations where the cluster is annealed from a truly molten state with different cooling rates down to 1 K. With a moderate cooling rate, the cluster is trapped in a smaller and smaller part of the phase space so that it describes a smooth caloric curve and smooth curves of for instance the radii of gyration versus temperature (see Figs. 3-5 in **Paper II**.) The glassy isomers found at 1 K

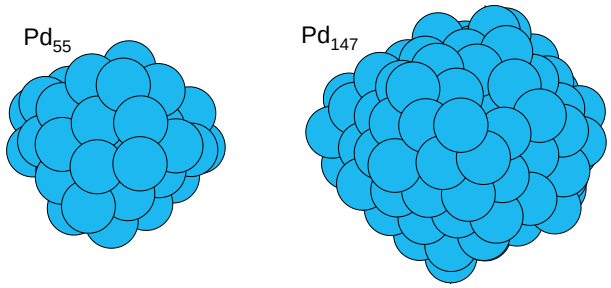


Figure 5.14: The drawings show the glassy isomers of $Pd_{55}$ and $Pd_{147}$ that are used as initial configurations in simulations of supercooled molten clusters.

by this procedure are depicted in Fig. 5.14. It must be noted that in the RSE simulations of the supercooled molten cluster, the cluster is probably not confined to the potential well of exactly one isomeric form but to many equivalent adjacent local minima separated with very small barriers. However, in the simulation at the lowest energy the supercooled cluster may be confined to only one or a few such isomers and since the total DOS curve is constructed by overlapping DOS curves with the fixed point at low energy, the total DOS approximately corresponds to a single isomer.

When these isomers are found RSE simulations are performed for the combination of the cluster with 55 and 147 oscillators, respectively. The original recipe [127] is that the reference system should have a DOS of similar magnitude as the examined system and we have found no reason to do differently. One complication is that the supercooled molten isomer tends to reshape to a structure with a lower potential energy and that the superheated cluster readily melts. A method to keep the cluster in a specific isomeric form in MD simulation has been proposed by Chekmarev and Krivov, [140]. We have simply interrupted the simulation when the cluster leaves the desired isomeric form.

The absolute DOS for $Pd_{147}$ for the different isomers and the caloric curves based on these DOS are illustrated in Fig. 5.15 and Fig. 5.16, respectively. At first we see that the DOS fairly captures the caloric curve of the supercooled molten cluster. The vertical line in Fig. 5.15 indicates the melting energy of $Pd_{147}$ calculated in the microcanonical simulations in **Paper II**. The reason why the RSE simulations yield a considerably higher melting energy is that the number of molten isomers must be included in the DOS of the molten phase and the DOS in Fig. 5.15 corresponds to only one molten isomeric form. In order to get a melting energy in agreement with the microcanonical simulations, the RSE simulations suggest that the number of equivalent molten isomers is $1.1 \cdot 10^{18}$ for $Pd_{55}$ and $4.1 \cdot 10^{41}$ for $Pd_{147}$.

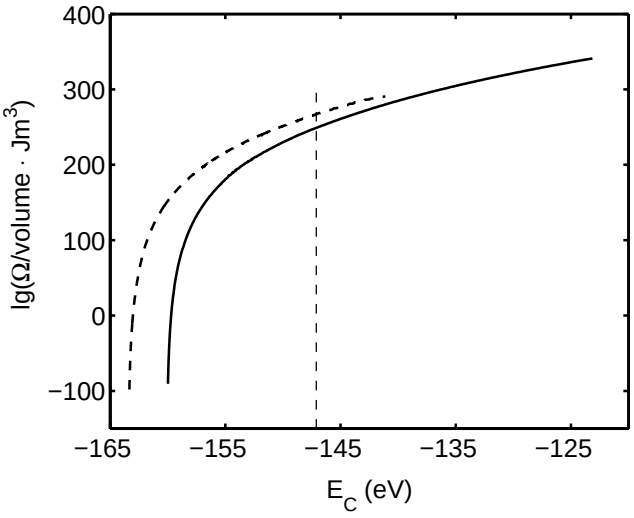


Figure 5.15: The graph shows the base ten logarithm of the absolute DOS for $Pd_{55}$ divided by the volume. The dashed curve represents the solid isomer and the solid curve represents the molten isomer.

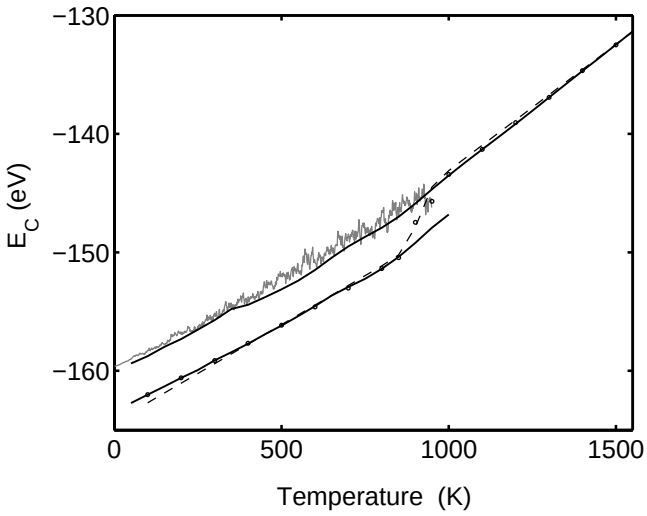


Figure 5.16: The caloric curve of $Pd_{55}$. Dashed line with dots: data from constant-temperature simulations. Upper solid lines: The caloric curve of molten isomer according to RSE DOS. Lower solid lines: The caloric curve of solid isomer according to RSE DOS. Jagged: The potential energy versus temperature in the annealing simulation.

## 5.4 Alternative techniques in cluster simulation

**J-walking and q-jumping Monte Carlo simulation** J-walking MC is used to overcome phase barriers in simulations [115, 141]. First a simulation is run at a high temperature $T_1$ which is sufficiently high so that the barrier is easily overcome. Then a simulation is run at a lower temperature $T_2$ at which the barrier may cause a quasiergodicity. However, in the latter simulation the system may every now and then try to rearrange from a configuration $\Gamma$ into a configuration $\Gamma_{T_1}$ generated at $T_1$. The probability for such a rearrangement is

$$probability = \min\left(1, \exp\left(\left(\frac{1}{k_B T_1} - \frac{1}{k_B T_2}\right)\left(E\left(\Gamma_{T_1}\right) - E\left(\Gamma\right)\right)\right)\right). \quad (5.3)$$

A modification of the J-walking MC method is the q-jumping MC method [142]. Similarly, configurations from a simulation at higher temperature are included in a simulation with quasiergodicity. It was found that the phase switches occurred more frequently using q-jumping than with ordinary canonical MC [142]. More methods of this kind can be found in Ref. [143].

**Finite time variation method** The Finite time variation (FTV) method is designed to obtain the free energy on the basis of canonical Monte Carlo simulations [144]. Let $H_{cluster}$ be the Hamiltonian that describes the cluster and that $H_{ref}$ is another Hamiltonian. The cluster described by $H_{cluster}$ is brought to equilibrium at a specific temperature and in the simulation the Hamiltonian is gradually changed from $H_{cluster}$ to $H_{ref}$. The change in free energy during the process $H_{cluster} \rightarrow H_{ref}$ can be calculated and thus the free energy difference to that of the reference state is obtained.

**The histogramming Monte Carlo method and the Multihistogram method** A method that is similar to RSE is the histogramming Monte Carlo method [49, 50]. In a canonical ensemble of the cluster, the probability of having the potential energy $U$ on the condition that the temperature is $T$ is

$$f\left(U\,|T\right) = constant \cdot \Omega_{pot}\left(U\right) \cdot \exp\left(-\frac{U}{k_B T}\right). \quad (5.4)$$

where $\Omega_{pot}\left(U\right)$ is the DOS of the potential energy. In a MC simulation at temperature $T$ the distribution $f\left(U\,|T\right)$ is obtained and $\Omega_{pot}\left(U\right)$ can be calculated apart from the constant. As in the RSE method the calculation $\Omega_{pot}\left(U\right)$ is accurate only for a narrow energy interval but with a number of simulations at different temperatures a continuous curve of $\Omega_{pot}\left(U\right)$ for a wide energy interval can be constructed. Subsequently the total DOS $\Omega\left(E\right)$ can be obtained by convolution of $\Omega_{pot}\left(U\right)$ and the analytically known DOS for the kinetic energy $\Omega_{kin}\left(E_{kin}\right)$ (see **Paper I**).

Even more similar to RSE is the multihistogram method [145, 146]. It is identical to the histogramming Monte Carlo method apart from that the MC simulations are run at constant energy.

# Part II

# Cooling and collisions

# Chapter 6

# Simulation details

## 6.1 Cluster-gas interaction

The interaction between each cluster atom and the gas atom in the collisions has been modeled by the Lennard-Jones potential

$$U(r_j) = 4\epsilon \left( \left( \frac{\sigma}{r_j} \right)^{12} - \left( \frac{\sigma}{r_j} \right)^{6} \right), \qquad j = 1, ..., n. \tag{6.1}$$

where $r_j$ is the distance between the gas atom and cluster atom number $j$. In **Paper III**, the He-He parameters were used to describe the interaction Pd-He. These parameters underestimate the interaction. Instead, in **Papers IV-VII** the interaction was approximated by the interaction between Xe (which is the rare gas atom in the same row of the periodic table as Pd) and the colliding rare gas. Subsequently, the Xe-gas parameters were estimated by the Lorents-Berthelot rules [147]:

$$\sigma_{He-Xe} = (\sigma_{He-He} + \sigma_{Xe-Xe})/2 \tag{6.2}$$

$$\epsilon_{He-Xe} = \sqrt{\epsilon_{He-He}\epsilon_{Xe-Xe}} \tag{6.3}$$

The well depth influences the energy transfer in collisions by accelerating the gas atom before the collision and possibly causing multiple-encounters. Of importance for the collisions is also the hardness (derivative) of the potential in the very hit. In simulations of collisions of large argon cluster on a platinum surface, Svanberg and Pettersson [148] found that the tail of the potential is of importance for the fragmentation dynamics. In their case, the Lennard-Jones potential described the long-range interaction better than the Morse potential.

For the integration of the equations of motions we have used the Runge-Kutta fourth order algorithm [149] with the timestep 0.5, 0.5, 0.75 and 1.0 fs for the collisions of Pd-clusters with He, Ne, Ar and Kr, respectively. The total energy is conserved to at least $10^{-5}$ eV. The MD program was originally written by Seong-Gon Kim.

## 6.2 Generation of initial coordinates and velocities

Collisions between $Pd_{13}$ and various rare gas atoms have been simulated. The rare gases have been He, Ne, Ar and Kr. Also a few simulations for $Pd_{55}$ were performed. The very shallow and short-range He-He interaction in **Paper III** made the collisions of almost hard-sphere character. It is therefore not certain that the trends observed can be extrapolated to collisions where the gas-cluster interaction is stronger. The main aim of the simulations was to calculate the average energy transfer at the gas temperature $T_g$ and the cluster temperature $T_c$. Later, a need to calculate the average energy transfer at $T_g$ and diverse internal, $T_{int}$, and translational temperatures, $T_{trans}$, of the cluster arose.

In an ensemble of realistic collisions at the temperatures $T_g$, $T_{trans}$ and $T_{int}$, the following parameters are described by distribution functions.
*i.* The initial cluster coordinate configuration, $\mathbf{R} = [x_1, y_1, z_1, x_2, ..., z_n]$, is distributed according to the Boltzmann distribution

$$f(\mathbf{R}) \propto \exp\left(-\frac{U(\mathbf{R})}{k_B T_{int}}\right), \tag{6.4}$$

where $U(\mathbf{R})$ is the potential energy of the configuration.
*ii.* The initial internal velocity in the $x$ direction of an atom in the cluster should be sampled according to the Maxwell-Boltzmann distribution

$$f(v_{x,j}) \propto \exp\left(-\frac{m_{Pd} v_{x,j}^2}{2 k_B T_{int}}\right), \qquad j = 1, ..., 13, \tag{6.5}$$

with a subsequent subtraction of the centre of mass velocity. Here $m_{Pd}$ is the mass of one palladium atom. Analogous sampling applies for the $y$ and $z$ directions. *iii.* The initial relative speed $v_R$ of the gas and the cluster is distributed according to

$$f_{v_R}(v_R) \propto v_R^3 \exp\left(-\frac{\alpha v_R^2}{2 k_B}\right), \tag{6.6}$$

where

$$\alpha = \frac{\frac{m_g}{T_g}\frac{m_c}{T_{trans}}}{\frac{m_g}{T_g} + \frac{m_c}{T_{trans}}}. \tag{6.7}$$

Here $m_g$ and $m_c$ are the gas and cluster masses, respectively.
*iv.* The gas atom should be placed so that the impact parameter $b$ is distributed according to

$$f_b(b) = \frac{2b}{b_{max}^2}, \tag{6.8}$$

where $b_{max}$ is the maximal $b$ for which the collision occurs.

In the simulations the distributions $f_b(b)$ and $f_{v_R}(v_R)$ for the generation of $b$ and $v_R$ have, for reasons of sampling efficiency been replaced by $\tilde{f}_b(b)$ and $\tilde{f}_{v_R}(v_R)$. The modified distribution of $b$ is defined as

$$\tilde{f}_b(b) = \begin{cases} 2\gamma & 0 < b < b_1 \\ \gamma & b_1 < b < b_{max} \\ 0 & b_{max} < b \end{cases} . \tag{6.9}$$

The value of $\gamma$ is given by the normalization condition on $\tilde{f}_b(b)$. The reason for the use of $\tilde{f}_b(b)$ is that more collisions are then simulated for small $b$, for which the energy transfer is most significant. In the calculation of the average energy transfer, the weight factor $f_b(b)/\tilde{f}_b(b)$ will compensate for not using $f_b(b)$ for the generation of $b$.

The distribution $\tilde{f}_R(v_R)$ is linear in $v_R^2$ and normalized and is a compromise between the distributions in Eq. 6.6 in the temperature intervals 100 K $< T_g <$ 900 K and 100 K $< T_{trans} <$ 1100 K (See Fig. 2 in **Paper VI**).

The advantage gained by the use of $\tilde{f}_R(v_R)$ is that it can be defined to be independent of the temperatures. By use of the weight factor $f_R(v_R)/\tilde{f}_R(v_R)$ that depends of the temperatures, the same set of collisions can be used to calculate the average energy transfer for various temperatures. In contrast, one set of simulations must be run for each $T_{int}$, since the distribution of the initial internal configuration of the cluster corresponds to a unique internal temperature.

In unimolecular chemical reactions, it is the internal excitation that determines the reaction rate [54]. The translational temperature is not directly relevant. However, in order to obtain zero energy transfer when the gas and the cluster are at equal temperature, the energy transfer to the translational mode of the cluster must be included. Consequently, the translation of the cluster before the collision must be known. The energy transfer *to* the cluster as well as to the translational and internal degrees of freedom, respectively, can be calculated for the collision $i$ as

$$\Delta E_{tot,i} = -\frac{m_g}{2}\left((\mathbf{v}_{g,i} + \Delta\mathbf{v}_{g,i})^2 - \mathbf{v}_{g,i}^2\right) \tag{6.10}$$

$$\Delta E_{trans,i} = \frac{m_c}{2}\left((\mathbf{v}_{c,i} + \Delta\mathbf{v}_{c,i})^2 - \mathbf{v}_{c,i}^2\right) \tag{6.11}$$

$$\Delta E_{int,i} = \Delta E_{tot,i} - \Delta E_{trans,i} \tag{6.12}$$

Here $\mathbf{v}_g$ and $\mathbf{v}_c$ are the initial gas and cluster velocities, respectively, and $\Delta\mathbf{v}_g$ and $\Delta\mathbf{v}_c$ are the changes in gas and cluster velocities, respectively. (Note that in **Papers IV** and **VII**, the energy transfer is defined as *from* the cluster, i.e with opposite sign. Throughout this summary the energy transfer is considered to be *to* the cluster.) The dynamics of the collision and hence $\Delta\mathbf{v}_g$ and $\Delta\mathbf{v}_c$ are independent of the absolute initial velocities. Therefore the absolute velocities $\mathbf{v}_{c,i}$ and $\mathbf{v}_{g,i}$ may be generated for collision $i$ after the simulation has been run. The advantage is again that one set of collisions

can be used for the calculation of the average energy transfer for various $T_g$ and $T_{trans}$.

In computer experiments we found that, for a given relative velocity $\mathbf{v}_R$, the conditional distribution of the initial cluster translational velocity $\mathbf{v}_c$ is

$$f\left(\mathbf{v}_{c_\parallel}|\mathbf{v}_R\right) \propto \exp\left(-\frac{\left(\mathbf{v}_{c_\parallel}+\delta\mathbf{v}_R\right)^2}{2\lambda^2}\right) \tag{6.13}$$

$$f\left(\mathbf{v}_{c_\perp}|\mathbf{v}_R\right) \propto \exp\left(-\frac{\mathbf{v}_{c_\perp}^2}{2\lambda^2}\right) \tag{6.14}$$

where

$$\delta = \frac{\frac{m_g}{T_g}}{\frac{m_g}{T_g}+\frac{m_c}{T_{trans}}} \tag{6.15}$$

and

$$\lambda = \sqrt{\frac{k_B}{\frac{m_g}{T_g}+\frac{m_c}{T_{trans}}}}. \tag{6.16}$$

$\mathbf{v}_{c_\parallel}$ is the component of $\mathbf{v}_c$ parallel to $\mathbf{v}_R$ and $\mathbf{v}_{c_\perp} = \mathbf{v}_c - \mathbf{v}_{c_\parallel}$ is the component of $\mathbf{v}_c$ perpendicular to $\mathbf{v}_R$. By simulation of $N$ collisions, the average energy transfer at the temperatures $T_g$, $T_{trans}$ and $T_{int}$ may now be calculated by

$$\begin{aligned}
\langle\Delta E\rangle_{T_g,T_{trans},T_{int}} &= \int_0^\infty\int_0^{b_{max}} \langle\Delta E\rangle_{b,v_R}\cdot f_b(b)\, f_R(v_R)\, db dv_R \\
&= \int_0^\infty\int_0^{b_{max}} \langle\Delta E\rangle_{b,v_R}\cdot \underbrace{\frac{f_b(b)\, f_R(v_R)}{\tilde{f}_b(b)\,\tilde{f}_R(v_R)}}_{g(b,v_R)} \tilde{f}_b(b)\,\tilde{f}_R(v_R)\, db dv_R \\
&\approx \frac{\sum_i^N \Delta E_i\cdot g(b_i,v_{R,i})}{\sum_i^N g(b_i,v_{R,i})}.
\end{aligned} \tag{6.17}$$

Especially, the energy transfer for collisions with impact parameter in the range $b' < b < b''$ is obtained by

$$\langle\Delta E\rangle_{T_g,T_{trans},T_{int},b} \approx \frac{\sum_i^{N_b} \Delta E_i\cdot g(b_i,v_{R,i})}{\sum_i^{N_b} g(b_i,v_{R,i})}, \tag{6.18}$$

where the $N_b$ collisions with $b' < b < b''$ are included in the sums.

# Chapter 7

# Categories of collision trajectories

## 7.1 Single encounter collisions

In contrast to other simulations related to unimolecular reaction rates [150] the cooling simulations for our clusters require the energy transfer close to equilibrium. Our simulations are therefore performed in temperature ranges around the equilibrium. In the simulations we have observed three classes of trajectories. The first and second are for single-encounter collisions. The trajectories with very small $b$ and with large $b$ differ in character. The first intriguing phenomenon is that collisions with small $b$ tend to heat the internal temperature of the cluster but collisions aiming further out tend to cool the cluster. The average energy transfer versus $b$ in collisions of the type $Pd_{13}$–Ne and $Pd_{13}$–Kr are shown in Fig. 7.1. To our knowledge this phenomenon has not previously been reported. The reason why only non-crossing curves have been reported before [51, 151, 152], we suppose, is because the temperature difference between the colliding species was too large. The phenomenon is only visible for the internal degrees of freedom. The translational energy transfer is constantly zero for all $b$ when $T_g = T_c$.

One fundamental necessity of molecular dynamics simulation is that the results should be time reversal invariant. Thus, if all the trajectories were to be run time reversed the average results should be the same if the gas and the cluster are in equilibrium. Since the cluster heating trajectories with small $b$ will become cluster cooling trajectories when time is reversed, these trajectories must start with a larger $b$ in the reversed direction. Consequently, trajectories with small initial $b$ must end up with, on average, a larger $b$ and vice versa. This has indeed been shown to be the case for the $Pd_{13}$–Kr collisions. (Fig. 9 in **Paper VI**).

The two classes of trajectories can also be distinguished by the way the gas atom velocity direction changes in the course of the collision. The average angle, $\varphi$, between the initial and final velocity of the gas atom is calculated for various impact parameters. A second average of the angle, $\varphi_s$, is defined

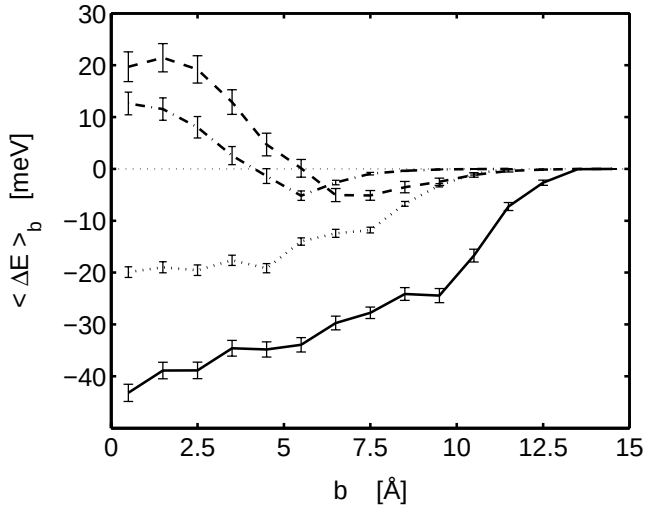


Figure 7.1: The graph shows the average energy transfer versus $b$ in collisions with $Pd_{13}$ at $T_c = 700$ K. The errorbars show 95 % confidence intervals. Solid curve: Kr, $T_g = 100$ K, Dotted: Ne, $T_g = 100$ K, Dashed: Kr, $T_g = 700$ K, Dashed-dotted: Ne, $T_g = 700$ K.

by considering an angle to be positive if the gas atom is bent towards the cluster and else negative. The two averages $\varphi$ and $\varphi_s$ are drawn for collisions between $Pd_{13}$ and Kr at $T_g = T_c = 700$ K in Fig. 7.2. For small $b$, the encounter is hard and the gas atom bounces off the cluster, leading to a large $\varphi$ and a negative $\varphi_s$. For very large $b$ we find that $\varphi = 0$ because the gas atom passes the cluster without notice. In between, however, $\varphi_s$ is positive, indicating that the gas atoms are attracted by the cluster but never really experience the repulsive forces near the cluster.

The different character of the trajectories can also be found in the change of cluster angular momentum $J = |\mathbf{J}|$, where

$$\mathbf{J}(\mathbf{R}) = \sum_{i=1}^{n} m_i \mathbf{x}_i \times \mathbf{v}_i \tag{7.1}$$

Here $\mathbf{x}_i$ and $\mathbf{v}_i$ are the position and velocity of cluster atom $i$. When $T_g = T_c$ the net change in $J$ is zero. However, collisions with small $b$ excite $J$ but larger $b$ leads to a cooling of $J$. (Fig 11 in **Paper VI**).

The change in $b$ in the course of a collision is in agreement with $\varphi_s$. When $b$ is very small, the gas atom bounces off and since the collisions are rather chaotic the outgoing $b$ will on average be larger than the incoming $b$. For larger initial $b$, the net attraction of the gas atom causes $b$ to decrease. This effect was found for all the gases He, Ne, Ar and Kr to approximately the same extent. The attraction of the gas atom is however not the only reason for the average decrease in $b$. A few simulations were run where the gas-cluster potential was changed into hard-sphere character. Although the gas

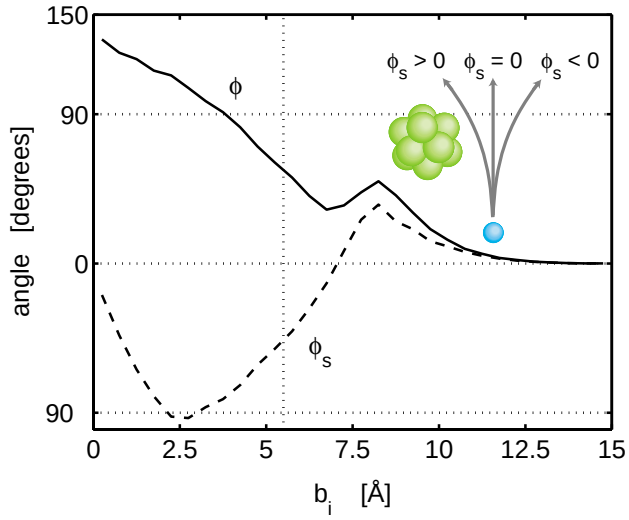


Figure 7.2: The graph shows the average angle between the initial and final velocity of the gas atom as a function of the initial impact parameters. In the dotted curve an angle is counted as positive if the gas atom is bent towards the cluster and negative if it is bent away.

atom experienced no attraction to the cluster, $b$ decreased on average for large $b$ and the energy transfer still had the same shape as in Fig. 7.1.

The curves of the energy transfer versus $b$ are mostly found to exhibit a plateau for small $b$, followed by a steep decrease and a tail [51, 151, 152, 153]. The difference between those earlier simulations and ours is that we have used a small difference in temperature between the colliding species. Even in our simulations the cross over phenomenon in the energy transfer was only observed near thermal equilibrium.

## 7.2 Multiple encounters and sticking

The third class of collisions that we have observed consists of multiple encounter and sticking collisions. If the energy of the incoming gas atom is very low, a possible loss of its energy might lead to the result that the gas atom cannot escape the cluster. In such a case, the gas atom will be reflected by the potential well and return for a second encounter. As long as the complex does not evaporate cluster atoms or collide with a third body, an energy fluctuation will eventually eject the gas atom. Still, if the lifetime of the complex is long, the corresponding capture is called sticking. The phenomenon is closely related to sticking on bulk surfaces [52, 53, 154]. Baule, one of the pioneers in energy transfer studies, vividly expressed sticking in 1914 as follows [157].

Manche Moleküle werden einmal, manche zweimal, manche

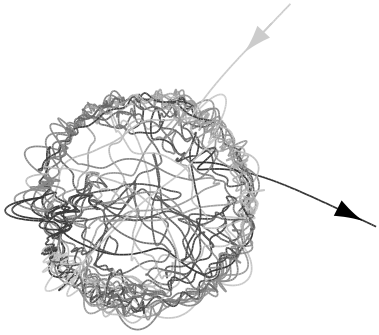

Figure 7.3: A collision between $Pd_{13}$ and Ar is shown. The argon atom finally leaves the cluster after 795 encounters with palladium clusters and 733 ps.

> öfter mit einem Molekül des festen Körpers zusammenrennen, ehe sie in den Gasraum zurückkehren, ja, manche Moleküle werden in das Innere des festen Körpers eindringen und erst, nachdem sie lange Zeit zwischen seinen Molekülen hin und her geworfen sind, das Freie wiederfinden.

Sticking is also of interest in cluster reactivity research [45, 155]. In the most extreme trajectory that we have observed, an argon atom performed 795 encounters before leaving the palladium cluster. The collision lasted for 733 ps. The trajectory is found in Fig. 7.3. The cluster temperature is 100 K and the initial relative speed in this collision equals the mean relative speed at $T_g = 65$ K. Each extra encounter in a collision leads in general to extra energy transfer. Thus, multiple encounters increase the energy transfer efficiency for the whole collision. In other words, the energy transfer efficiency is likely to be higher for cold gas than for warm gas. In Fig. 7.4. the distance from the argon to the nearest palladium atom is drawn versus time. This figure illustrates how the energy of the colliding complex fluctuates. At about 375 ps the gas atom has gained energy from the cluster and is almost escaping. However, in the preceding encounters, energy is given back to the cluster. Not until at 733 ps does an energy fluctuation lead to the escape of the argon atom. The grey scale of the three-dimensional trajectory in Fig. 7.3 shows a gas atom that irregularly jumps over the cluster surface. Thus, the gas atom is not stuck to a specific palladium atom or a cluster site.

The potential well between a surface of a bulk solid or a cluster and for instance an $N_2$ molecule shows two distinct minima. A more shallow well further out from the surface and one deeper, close to the surface. They represent physisorption and chemisorption, respectively [107]. In physisorption the gain in energy is due to dispersion attraction between surface and adsorbate, but chemisorption is due to electron transfer between surface and adsorbate [59, 156]. The Lennard-Jones potential can only describe pysisorption, since it represents interaction due to dispersion attraction. Hence, physisorption is the only kind of sticking that we have observed but since the rare gas atoms

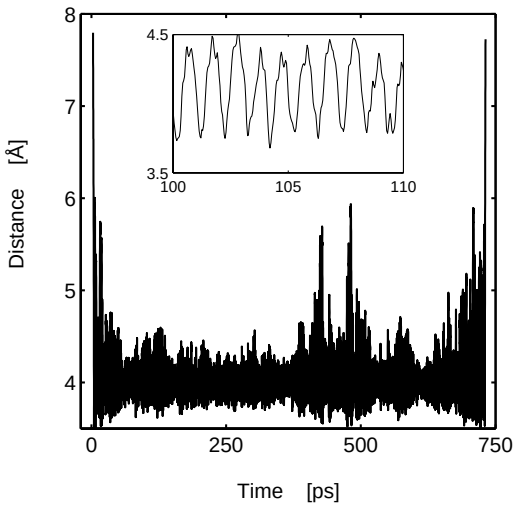


Figure 7.4: The distance from the argon atom to the nearest palladium atom is shown as a function of time for the trajectory in Fig. 7.3. A magnification of a small part of the curve is shown in the inset.

are inert, the Lennard-Jones potential is sufficient. To study chemisorption more advanced analytical potentials [34] or *ab initio* calculations are required [158, 159, 160].

# Chapter 8

# Energy transfer

## 8.1 Statistical models

The average energy transfer per collision between $Pd_{13}$ and the He, Ne, Ar and Kr atoms is shown in Figs. 8.1 and 8.2. Both figures show the typical behaviour of the average energy transfer. First, in the figure with fixed cluster temperature and varying gas temperature $T_g$, all the curves turn linear at high $T_g$. At high gas temperature, the collisions are to a large extent of single-encounter type and the energy transfer is a linear function $\langle \Delta E \rangle \sim k\,(T_g - T_c)$. At low gas temperature the energy transfer exceeds the linearity due to multiple-encounter character of the collisions. In the second figure with fixed gas temperature, the energy transfer is a linear function of $T_c$ but increases in efficiency at higher temperatures. The increasing efficiency is due to the increasing softness and eventual melting of the cluster. In **Paper III**, collisions with "softer" intra-cluster potential parameters were studied. The simulations showed that the softer the vibrations were within the cluster, the more efficient was the energy transfer.

The figures suggest that the energy transfer might be modeled by a simple proportionality to $T_g - T_c$, at least for a single *encounter*. The energy transfer per *collision* at low temperature might then be explained by the presence of multiple encounters. In the following sections the energy transfer of the simulations will be analyzed using three statistical models developed by Nordholm and co-workers [86, 87, 88].

## 8.2 Collision cross section

One of the common features of the statistical models is that the energy transfer in a collision is assumed to be independent of the impact parameter apart from the distinction between "hits and misses". This distinction is implied by the definition of the cross section. In contrast, in simulated collisions, the character of a collision is very much dependent on the actual value of the impact parameter. Even the separation between hits and misses

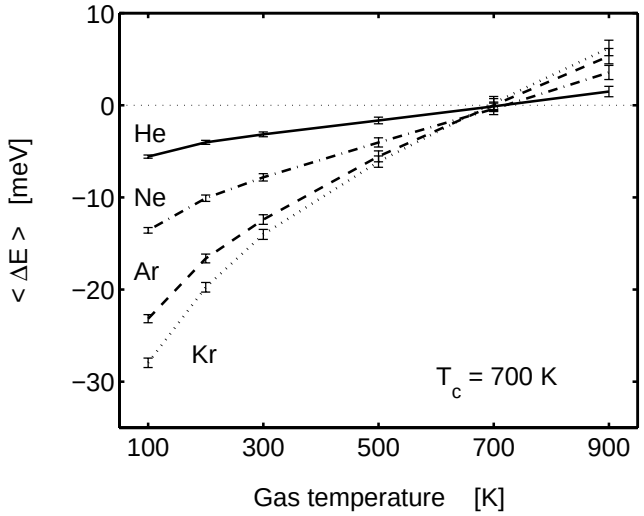


Figure 8.1: The average energy transfer to $Pd_{13}$ is shown for collisions with He (solid curve), Ne (dashed-dotted), Ar (dashed) and Kr (dotted). The cluster temperature is 700 K. The errorbars show 95 % confidence interval.

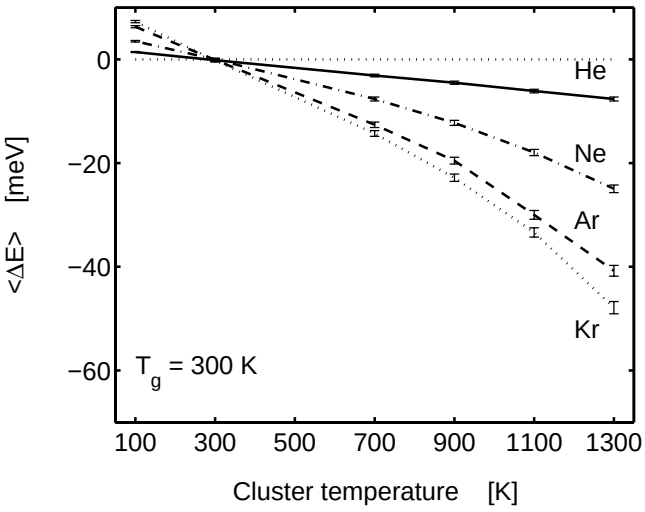


Figure 8.2: The average energy transfer to $Pd_{13}$ is shown for collisions with He (solid curve), Ne (dashed-dotted), Ar (dashed) and Kr (dotted). The gas temperature is 300 K. The errorbars show 95 % confidence interval.

is arbitrary in simulation as the energy transfer is strictly non-zero for any impact parameter according to classical mechanics when potentials such as our chosen Lennard-Jones interaction are used. Since the energy transfer decreases with $b$ (in unpublished calculations we have found that the energy transfer decreases as $b^{-12}$ for large $b$ when the gas-cluster interaction is of Lennard-Jones (12-6) character), the average energy transfer depends on at what $b$-value trajectories will be split into hits and misses. When comparing data from simulations with the predictions of the statistical models, a realistic collision cross section must therefore be used.

In collisions where the temperatures of the colliding species are very different, the energy transfer versus $b$ often shows a plateau for small $b$, followed by a steep decrease and a long (infinite) tail [51, 151, 161, 152, 162] An intuitive choice of realistic cross section is then defined by an impact parameter cut-off approximately where the tail starts. However, when $T_g \approx T_c$ the energy transfer versus $b$ will change from positive to negative before it approaches zero for large $b$, as seen in Fig. 7.1. Instead of using the $\langle \Delta E \rangle$ versus $b$ curve for cross section estimations, we have used the $\langle b\,|\Delta E| \rangle$ versus $b$ curve. The energy transfer, regardless of sign, is a measure of the strength of the gas-cluster interaction. In Fig. 8.3, the curve $\langle b\,|\Delta E| \rangle$ versus $b$ is drawn for $Pd_{13}$ colliding with Kr and Ne atoms at $T_g = T_c = 700$ K. These curves are now used to define a proper collision cross section. The cross section radius, $csr = \sqrt{\text{cross section } /\pi}$, of the collisions we define by the relation

$$\frac{\int_0^{csr} \langle b\,|\Delta E| \rangle\, db}{\int_0^{\infty} \langle b\,|\Delta E| \rangle\, db} = 0.95. \tag{8.1}$$

Such a definition is of course arbitrary to some degree.

The cross section radius varies only a few percent with cluster temperature but is more sensitive to the gas temperature. In Fig. 8.4, $csr$ at $T_c = 700$ K is drawn for various gas temperatures and different gases. The cross section radius increases significantly with decreasing gas temperature. This result is not surprising. When the gas temperature is low, i.e. the gas atom speed is on average low, the attraction of the potential can capture gas atoms for far larger impact parameters than in the case of high $T_g$. The energy transfer results presented in **Papers VI** and **VII** are related to this definition of the cross section. In **Papers III-V** a fixed cross section of 6.5 Å was used.

## 8.3 ECT

In the Ergodic Collision Theory [86] each collision is assumed to lead to microcanonical equilibrium between the two colliding species. The energy of the incoming gas atom is on average $\langle E_g \rangle = 3k_B T_g/2$ and the energy

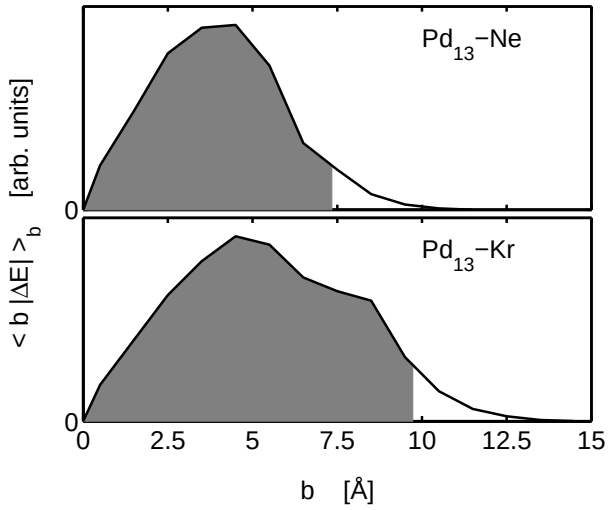


Figure 8.3: $\langle b\,|\Delta E|\rangle$ versus $b$ for collisions with Kr and Ne. The gas and cluster temperatures are each 700 K. The shaded areas show 95% of the total areas.

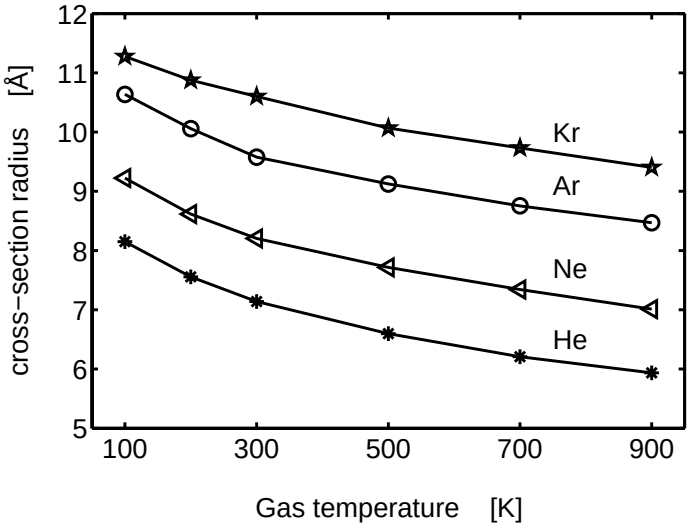


Figure 8.4: The graphs shows the collision cross section radii versus gas temperature according to the definition in Eq. 8.1. The collisions are between $Pd_{13}$ at $T_c = 700$ K and Kr (pentagrams), Ar (rings), Ne (triangles) and He (stars).

of the cluster is $\langle E_c \rangle = f(T_c)$, which is the caloric curve in Fig. 5.1. The microcanonical equilibrium established in the collision is written as an energy balance,

$$3k_B T_g/2 + f(T_c) = 3k_B T'/2 + f(T'). \tag{8.2}$$

The heat capacity is considerably larger for the cluster than for the gas atom and thus a single collision will change the cluster temperature only slightly. We can approximate $f(T') - f(T_c) \approx C(T_c)(T' - T_c)$, where $C$ is the heat capacity of the cluster. Using Eq. 8.2, the ECT energy transfer is found to be

$$\langle \Delta E \rangle_{ECT} = f(T') - f(T_c) = C(T_c) \frac{3k_B/2}{3k_B/2 + C(T_c)} (T_g - T_c). \tag{8.3}$$

The energy transfer in collisions of collisions with van der Waals interaction is normally far from complete in the ECT sense. The energy transfer efficiency can be described by the factor $\beta_E$ defined as

$$\beta_E = \frac{\langle \Delta E \rangle_{simulation}}{\langle \Delta E \rangle_{ECT}}. \tag{8.4}$$

In an investigation of highly energized organic molecules in collisions with small inorganic medium molecules, Börjesson *et al.* [163] found $\beta_E$ to be between 0.05 and 0.25. In Fig. 8.5, the efficiency factor is shown for collisions at $T_c = 700$ K. The first observation is that the efficiency is higher when the gas temperature is low as mentioned above. Secondly, in the single-encounter regime, the efficiency is independent of temperature and increases with increasing gas atom size. When the mass of the gas molecule is high, the collision event takes longer time which allows for a larger energy transfer. Furthermore, there is a Baule formula predicting increasing efficient energy transfer when the masses of colliding species approach each other [157, 164].

## 8.4 PECT

The very encounter of the gas atom and the cluster defined in terms of strong interaction is a rapid event and during the short period of energy transfer, only of few degrees of freedom participate. That is the starting-point of the Partially Ergodic Collision Theory (PECT) [87, 88]. In this theory microcanonical equilibrium is assumed to be established between subsets of $n$ degrees of freedom in the cluster and $m$ in the gas atom. The energy balance of the equilibrium is

$$mk_B T_g/2 + nk_B T_c/2 = (m+n) k_B T'/2, \tag{8.5}$$

and the energy transfer is

$$\langle \Delta E \rangle_{PECT} = \frac{mn}{2(m+n)} k_B (T_g - T_c). \tag{8.6}$$

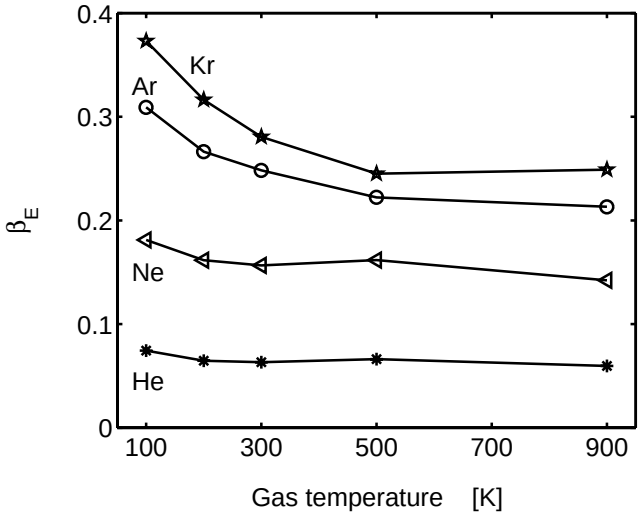


Figure 8.5: The graph shows the energy transfer efficiency $\beta_E$ according to ECT versus gas temperature in collisions with $Pd_{13}$ at $T_c = 700$ K. Kr (pentagrams), Ar (rings), Ne (triangles) and He (stars).

Since the energy transfer efficiency increases with decreasing gas temperature, the PECT parameters $m$ and $n$ will increase with decreasing gas temperature. One reason can be that at low gas temperature the encounters are slower and more degrees of freedom can indeed participate. A second explanation is that the number of participating degrees of freedom have not increased at low gas temperature but the increased energy transfer efficiency of the collision is due to multiple encounters. The rare gas atoms have no internal degrees of freedom and if we assume that the only one of the translational degrees of freedom participates we should use $m = 1$. Solving the equation $\langle \Delta E \rangle_{PECT} = \langle \Delta E \rangle_{simulation}$ at $T_c = 700$ K and $T_g = 900$ K, we found $n = 0.2$, 0.7, 1.8 and 2.5 for He, Ne, Ar and Kr, respectively.

## 8.5 PEMET

It has been shown that statistical models that include the capture strength have a relatively higher predictive power than simpler models [153]. Such a model is the The Partially Ergodic Multiple Encounter Theory, PEMET, which was originally developed by Börjesson and Nordholm [87, 88]. When the gas atom is cold it might be trapped by a potential well at the cluster surface. This mechanism is supported by our simulations. In the extreme case as in Figs 7.3 and 7.4, the gas atom is trapped for a long time but in most multiple encounter collisions only a few encounters occur before the gas atom escapes. In PEMET a collision is thought of as a series of encounters ended by the escape of the atom (or generally, the gas molecule). In each encounter, microcanical equilibrium is established between $n$ and $m$ degrees

of freedom in the cluster and the gas atom, respectively. After the hit, the gas atom turns away from the cluster, but only if it has sufficient energy to climb the potential well between the cluster and the gas atom can it escape. If not, a total redistribution of energy within the cluster and within the gas atom is assumed before the gas atom comes around for a second hit. A more detailed description of PEMET is found in **Paper VII**.

PEMET includes many simplifications. First, the cluster-gas potential is assumed to be of square-well type with the depth $V_0$. Second, between each encounter the cluster and the gas atom is assumed to be fully relaxed. This approximation is supported by the fact that the time between each encounter is about 1 ps and during that time the cluster atoms in $Pd_{13}$ cover a few vibrations. Furthermore, the trajectory in Fig. 7.3, shows that the gas atom is constantly moving around the cluster surface, hitting new cluster atoms. Third, the escape probability is assumed to be determined by one degree of freedom. If the temperature of the motion in that degree of freedom is $T$, the probability of escape is

$$P_{esc} = \frac{\int_{V_0}^{\infty} E^{-1/2} \exp\left(-E/k_B T\right) dE}{\int_{0}^{\infty} E^{-1/2} \exp\left(-E/k_B T\right) dE} \tag{8.7}$$

Fourth, the parameters $n$ and $m$ are assumed to be temperature-independent.

A major problem in PEMET is to calculate the energy of the gas atom after escape. In the first encounter, the colliding degrees of freedom are heated by the binding energy corresponding to the potential well $V_0$. Therefore, even at $T_g = T_c$, energy will be transferred from the active degrees of freedom to the cluster. This leakage must be regained by the gas atom at escape. Physically this is assured since the gas atoms that manage to escape have a higher energy than average. (Compare with the cooling effect by water evaporating from the skin.) However, we have not been able to create a physically realistic, quantitative model that leads to zero energy transfer when $T_g = T_c$. Instead, a completely empirical compensation term has been added to the escape energy in order to assure equilibrium

There are two features we want to be reproduced by PEMET. First, the energy transfer versus gas temperature curves in Fig. 8.1. Second, from the simulations we have drawn histograms of number of encounters per collision. Such histograms should be satisfyingly reproduced by PEMET.

The PEMET energy transfer has been fitted to simulation data in the least square sense at $T_c = 100$ K and 700 K, respectively. As in the PECT calculations we set $m = 1$. The optimal parameters are found in Table 1 in **Paper VII**. $Q_{T_c}$ in this table is the average deviation between PEMET and simulations. Note that the reason why $Q_{T_c}$ is relatively small for helium is that so is the average energy transfer for helium. The average energy transfer from simulation as well as from the PEMET fits are drawn for collisions with argon in Fig. 8.6. We observe that the PEMET predicts accurately the increased energy transfer for low gas temperature. Furthermore the PEMET

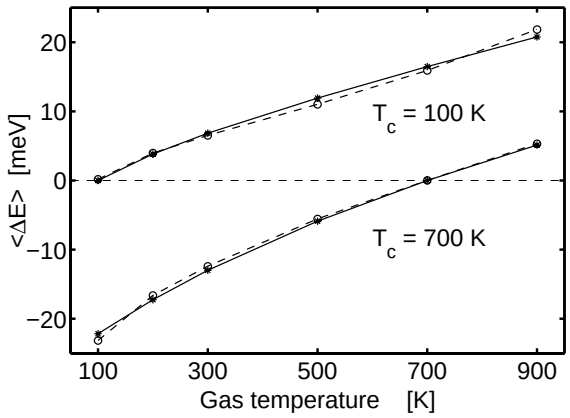


Figure 8.6: The graph shows the average energy transfer in $Pd_{13}$-Ar collisions as a function of gas temperature. The cluster temperature is 100 K (upper curves) and 700 K (lower curves) respectively. The dashed curves with rings are from simulations and the solid curves with stars are from PEMET fits.

parameters imply that multiple-encounter collisions are more frequent for krypton than for helium.

The distributions of number of encounters per collision in Fig. 8.7 show that the PEMET only qualitatitvely describes the collisions. The bars are from simulations and the curves are from PEMET. More multiple encounters occur at the low gas temperatures (black bars and dashed curves) than at the high gas temperatures. This is indeed reproduced by PEMET. However, PEMET predicts in all cases a higher frequency of multiple encounters than simulations. We can conclude that PEMET qualitatively describes the collisions. However, multiple encounters are overestimated due to the underestimation of the escape probability in Eq. 8.7. At high temperatures, the escape probability should be almost unity.

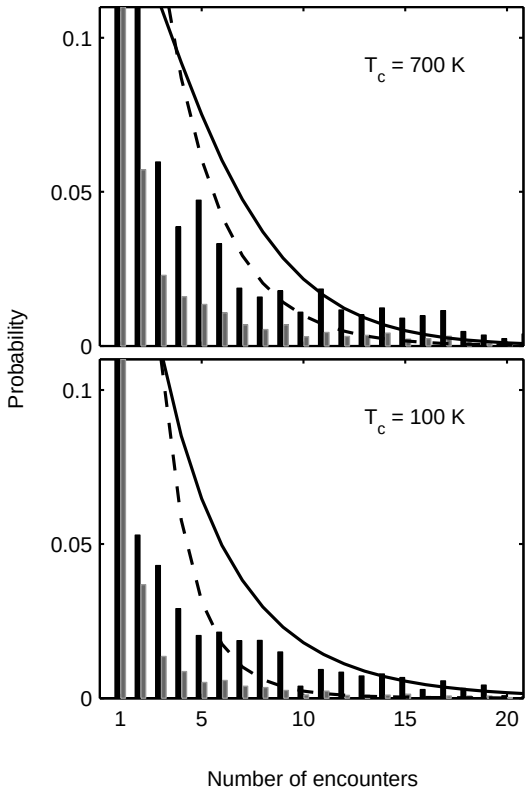


Figure 8.7: Histograms over the number of encounters per collision in collisions of $Pd_{13}$ and Ar are shown. (Upper panel) $T_c = 700$ K. The bars show simulation data and the curves PEMET calculations. The black bars and the solid curve corresponds to $T_g = 100$ K and the grey bars and the dashed curve corresponds to $T_g = 500$ K. (Lower panel). The same as above but $T_c = 100$ K.

# Chapter 9

# Cooling of clusters in a rare gas atmosphere

Hot clusters may cool by evaporation of atoms, ejection of electrons, photon radiation and by collisions with a surrounding gas [165]. Only the latter aspect will be treated here. The simulation scheme in **Paper VI** was originally developed to be able to use one set of simulations for different gas temperatures. The cluster temperature must be fixed as the spatial configurations of the cluster correspond to a certain $T_c$. In the cooling of a cluster from an initially high temperature $T_c(0)$ to the lower gas atmosphere temperature $T_g$, we observed that the translational temperature of the cluster, $T_{trans}$, decays much quicker than the internal temperature, $T_{int}$. Hence, a proper study of the cooling requires data of the energy transfer at different $T_{trans}$ and $T_{int}$. Fortunately, the internal cluster temperature only enters the simulation scheme in the internal configuration of the cluster and one set of simulations can be used to calculate the energy transfer for varying $T_g$ and $T_{trans}$. Only $T_{int}$ is fixed.

The rate of change in temperature is proportional to the collision frequency, $z(T_{trans}, T_g)$, the energy transfer, $\langle \Delta E_{trans} \rangle_{T_g, T_{trans}, T_{int}}$ and $\langle \Delta E_{int} \rangle_{T_g, T_{trans}, T_{int}}$, respectively, and inversely proportional to the cluster heat capacity of the translational degrees of freedom, $c_{trans}(T_{trans})$, and internal degrees of freedom, $c_{int}(T_{int})$, respectively. The cooling of the cluster temperatures $T_{trans}$ and $T_{int}$ is modeled by a system of coupled differential equations.

$$\begin{cases} dT_{trans}/dt = \langle \Delta E_{trans} \rangle_{T_g, T_{trans}, T_{int}} \cdot z(T_{trans}, T_g) / c_{trans}(T_{trans}) \\ dT_{int}/dt = \langle \Delta E_{int} \rangle_{T_g, T_{trans}, T_{int}} \cdot z(T_{trans}, T_g) / c_{int}(T_{int}) \end{cases} \tag{9.1}$$

The collision frequency is an analytical function of temperatures, gas masses and the gas pressure. The energy transfer is taken from the collision simulations and the heat capacity is taken from the MC simulations in **Paper I**. The collision frequency depends on the collision cross section but so does the average energy transfer and the dependencies cancel in Eq. 9.1. The only function of the pressure is to determine the time scale of the cooling.

In Fig. 9.1 the cooling of the cluster from 1300 K in an atmosphere of neon at 100 K and 300 K, respectively, is shown. The curves are similar in shape for the other rare gases in the study. As assumed, the cooling rate of the cluster translation is much higher than that for the internal degrees of freedom. Thus, only a negligible error is introduced if we assume that the translation of the cluster is immediately thermalized to the gas temperature. Consequently, only the energy transfer to the internal degrees of freedom are of importance. However, the translational degrees of freedom does take an active part in the energy transfer in the sense that cold translational degrees of freedom contribute to the cooling of the internal degrees of freedom of the cluster.

In **Papers III-V**, the cooling was not just calculated using energy transfer data, heat capacity data and the cooling equation but simulations of the cooling were performed as well. In such simulations one hot cluster was allowed to collide with gas atoms in many consecutive collisions and the temperture was followed as a function of the number of collisions. The cooling rate in such simulations agreed well with the cooling predicted by the cooling equation.

A realistic pressure in the cluster source in a cluster experiment might be 100 mbar. With this pressure we found that the cooling time required is less than half a microsecond. With this a as guide it should be possible to design an experimental setup so that the cluster is fully thermalized by a gas. Among the rare gases, we find that argon and krypton are the best cooling agents.

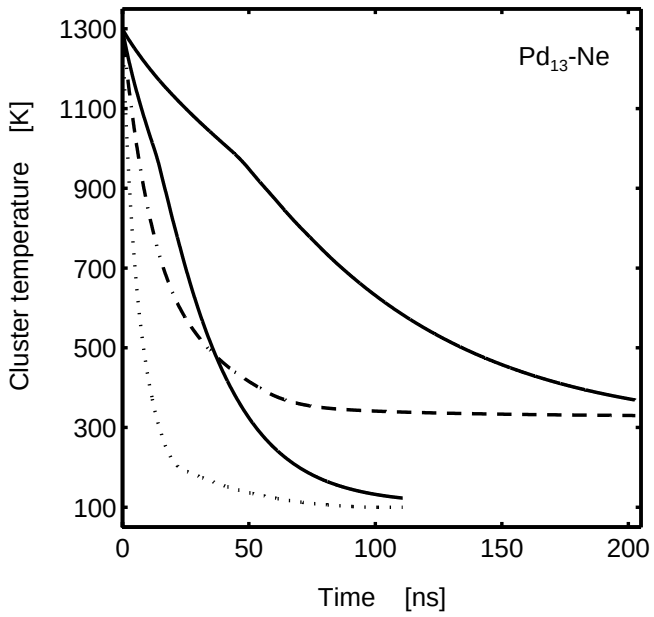


Figure 9.1: The temperature decay of a $Pd_{13}$ cluster in a neon atmosphere of 100 mbar is shown. The initial cluster temperature is 1300 K. The solid curves show the internal temperature and the dashed/dotted ones show the translational temperature

# Chapter 10

# Discussion and outlook

Computer simulations are fascinating in that microscopic processes can be followed on a very detailed level. For the development of theories describing the melting in finite systems, mostly simulations of Lennard-Jones clusters have been used in the past. Many-body potentials have also been used with the aim to model metal clusters. When evaluating the merit of simulations there are two different types of accuracy to assess: i) the accuracy of the simulation results with respect to the chosen model and ii) the accuracy of the model with respect to the reality it tries to describe. Our results should at least be accurate in the former sense but perhaps not as accurate in the latter sense.

A new criterion of a non-fragmented cluster has been introduced for simulation of canonical systems. No restrictions were put on the shape of the cluster and indeed we found that small molten clusters are not spherical. In both the constant-temperature and constant-energy simulations the major problem with nonergodicity due to phase barriers was observed and the calculated melting points for the clusters $Pd_{54}$, $Pd_{55}$, $Pd_{147}$ and $Pd_{309}$ are therefore not reliable.

As a contribution to the solution we have presented Reference System Equilibration (RSE) simulations with the aim to calculate the absolute DOS for the clusters. In the case of $Pd_{13}$ the RSE method manage to reproduce the canonical caloric curve excellently over the whole temperature interval from 100 to 1600 K. One great advantage with the RSE method is that comparison with a known DOS for a calibration state of the cluster is required only if the absolute DOS is desired. Furthermore, with the choice of reference system to be independent harmonic oscillators, it is considerably less time-consuming to do one MC step with the reference system than with the cluster. Therefore a RSE simulation is not much more time-consuming than an ordinary canonical simulation.

The results from the RSE simulations of separated solid and molten isomers of $Pd_{55}$ and $Pd_{147}$ were encouraging but the number of statistically equivalent isomers must be known in order to reach the goal to calculate the melting point. However, in **Paper II** we initiate another strategy for the

calculation of the melting point. The molten phase of the cluster is confined to a sphere so that when the energy of the combined system increases the cluster approaches the hard-sphere fluid system for which the absolute DOS should be possible to determine on an absolute scale. We are looking forward to the completion of such a calculation.

Simulations of cluster-gas atom collisions have been used to calculate the energy transfer and with the aid from the heat capacity calculations a subsequent calculation of the cooling of the cluster in a rare gas atmosphere was performed. With the improved simulation scheme in **Paper VI**, the simulated collisions did satisfy the applicable equilibrium constraint. Many interesting phenomena could then be observed at equilibrium. With this simulation scheme, a considerably amount of information of high accuracy could be extracted from a single set of simulations. The cooling curves showed that indeed the translation is cooled much faster than the internal degrees of freedom.

One goal with using simulation is to investigate atomic systems in a way that is not possible in experiments. A fundamental understanding of mechanisms may be the major issue and quantitative agreement with experiments is then not of highest priority. However, in the industry today there is a need for simulations that should replace experiments in order to reduce costs. Are the simulations presented in this thesis of such accuracy that they could favourably be compared with experimental data? In the case of the melting point certainly not. There are two major things that reduce the accuracy: nonergodicity due to a phase barrier and inaccurate potential energy surface calculations. Methods to efficiently overcome barriers are of great need. There are promising methods available as the j-walking and q-jumping MC methods. Even more informative are however the methods that determine the density of states of systems. The calculation of the anharmonicity of vibrations in e.g. clusters is an exciting future research field. The anharmonicity is not only of interest for clusters but also for bulk materials as well as most molecular systems.

The potential energy surface of clusters has recently been calculated in *ab initio* studies of melting [166]. Eventually, with fast computers and optimized algorithms, such fundamental energy calculations will be the most accurate ones. It might however be questioned if enough configurations can be explored with these time-consuming calculations in order to achieve accurate statistics. For now the parametrized functionals probably give best results. An accurate potential for sodium clusters would be desireable in order to compare simulations with the experimantally known melting points.

A natural continuation of cluster-gas collisions would be to simulate collisions with reactive gases like CO and $O_2$. Such collisions with possible sticking and even chemisorption would certainly be of great interest.

# Acknowledgements

First of all I would like thank my wife Marie for her incredible patience. Being a PhD student unfortunately intrudes upon family life and without you I could of course not have brought this work to completion.
I also would like to thank my parents for being so supportive throughout my studies.
Thanks also go to my supervisor Prof. Arne Rosén. Few people are so enthusiastic and well-informed about science and especially new discoveries in science. My second supervisor has been Prof. Sture Nordholm to whom I am so grateful for all these hours of fruitful discussions on thermodynamics and for all your support.
During my time as a PhD student I have been fortunate to be in the Molecular Physics Group. Among its members and former members I would like to give special thanks to Henrik Grönbeck who tried to teach my to be very accurate in science; to Mats Andersson for supervising me in the laboratory, for being a nice companion on conferences and for being a great source of knowledge about science; to Nils Tarras-Wahlberg for a pleasant collaboration in the laboratory and to Leif Johansson for helping me with everything that did not work. I must not forget to mention all amusing discussions about everything in life with my room-mates Nils and Leif.
I am very happy for all the friends in the Molecular Physics group. Thank to Kim Bolton, Daniel Bozi, Alf-Peter Elg, Marica Ericson, Eva Eriksson, Michael Försth, Sofia Grapengiesser, Fredrik Gudmundson, Gunner Hanehøj, Lotta Holmgren, Birgitta Högman, Åsa Johansson, Johan Mellqvist, Fredrik Persson, John Persson, Anders Snis, Sven Varga, Erik Westin, Torbjörn Åklint and Daniel Östling.
Finally I would like to thank Nikola Markovic, Chalmers, and Anatoly Belonoshko, Uppsala University, for their important advice on simulation techniques.

# Bibliography


[1] W. Ekardt (ed.), "Metal Clusters", John Wiley & Sons, 1999

[2] H. Haberland (ed.), "Clusters of Atoms and Molecules I", Chemical Physics 52, Springer-Verlag, 1994

[3] H. Haberland (ed.), "Clusters of Atoms and Molecules II", Chemical Physics 56, Springer-Verlag, 1994

[4] J. Jellinek (ed.), "Theory of Atomic and Molecular Clusters", Springer, 1999

[5] M. Moskovits, "Metal Clusters", John Wiley & Sons, 1986

[6] A. Rosén, KOSMOS, 119 (1993)

[7] W. D. Knight, K. Clemenger, W. A. de Heer, W. A. Saunders, M. Y. Chou, M. L. Cohen, Phys. Rev. Lett. **52**, 2141 (1984)

[8] F. Chandezon, P. M. Hansen, C. Ristori, J. Pedersen, J. Westergaard and S. Bjørnholm, Chem. Phys. Lett. **277**, 450 (1997)

[9] T. P. Martin, S. Bjørnholm, J. Borggreen, C. Brechignac, Ph. Cahuzac, K. Hansen and J. Pedersen, Chem. Phys. Lett. **186**, 53 (1991)

F. Chandezon, P. M. Hansen, C. Ristori, J. Pedersen, J. Westergaard and S. Bjørnholm, Chem. Phys. Lett. **277**, 450 (1997)

[10] W. A. de Heer, P. Milani and A. Chatelain, Phys. Rev. Lett, **65**, 488 (1990); A. Hirt, D. Gerion, I. M. L. Billas, A. Châterlain and W. A. de Heer, Z. Phys. D, **40**, 160 (1997)

[11] M. B. Knickelbein, Chem. Phys. Lett. **192**,129 (1992)

[12] R. Kusche, Th. Hippler, M. Schmidt, B. von Issendorff and H. Haberland, Eur. Phys. J. D, **9**, 1 (1999)

[13] K.-H. Meiwes-Broer, "Metal Clusters at Surfaces", Springer, 2000

[14] H. Haberland, M. Moseler, Y. Qiang, O. Rattunde, Th. Reiners and Y. Thurner, Surface Review and Letters, Vol. **3**, **1**, 887 (1996)

[15] S. J. Caroll, S. Pratontep, M. Streun, R. E. Palmer, S. Hobday and R. Smith, J. Chem. Phys. **113**, 7723 (2000)

[16] P. Fayet, F. Granzer, G. Hegenbart, E. Moisar, B. Pischel and L. Wöste, Phys. Rev. Lett. **55**, 3002 (1985); Z. Phys. D, **3**, 299 (1986)

U. Heiz, A. Sanchez, S. Abbet and W.-D. Schneider, J. Am. Chem. Soc. **121**, 3214 (1999)

[17] U. Heiz, A. Sanchez, S. Abbet and W.-D. Schneider, J. Am. Chem. Soc. **121**, 3214 (1999)

[18] A. Sanchez, S. Abbe, U. Heiz, W.-D. Schneider, H. Häkkinen, R. N. Barnett and U. Landmann, J. Phys. Chem. A, **103**, 9573 (1999)

[19] B. C. Gates, Chem Rev, **95**, 511 (1995)

[20] V. Depuis, J. P. Perez, J. Tuaillon, V. Paillard, P. Mélinon, A. Perez, B. Barbara, L. Thomas, S. Fayeulle and J. M. Gay, J. Appl. Phys. **76**, 10 (1994)

[21] J. P. Perez, V. Depuis, J. Tuaillon, A. Perez, V. Paillard, P. Mélinon, M. Treilleux, L. Thomas, B. Barbara, B. Bouchet-Fabre, J. Magn. Magn. mMter. **145**, 74 (1995)

[22] J. Bansmann, L. Lu, V. Senz, A. Bettac, M. Getzlaff and K.H. Meiwes-Broer, Eur. Phys. J. D, **9**, 461 (1999)

[23] C. Johansson, T. Åklint, M. Hanson, M. Andersson, N. Tarras-Wahlberg, E. Olsson, B Kalska, R. Wäppling and A. Rosén, NanoStructured Materials, **12**, 287 (1999)

[24] M. Homer, J.L. Persson, E.C. Honea, and R. L. Whetten, Z. Phys. D, **22**, 441 (1991)

[25] M. Kappes, M. Schär, U. Röthlisberger, C. Yeretzian, and E. Schumacher, Phys. Rev. Lett. **143**, 251 (1988)

[26] J. Akola, H. Häkkinen and M. Manninen, Eur. Phys. J. D, **9**, 179 (1999)

[27] L. Holmgren, M. Andersson, and A. Rosén, J. Chem. Phys. **109**, 3232 (1998)

[28] M. Schmidt, R. Kusche, W. Kronmüller, B. von Issendorff and H. Haberland, Phys. Rev. Lett. **79**, 99 (1997)

[29] M. Schmidt, R. Kusche, B. von Issendorff and H. Haberland, Nature, **393**, 238 (1998)

[30] R. von Pietrowski, M. Rutzen, K. von Haeften, S. Kakar and T. Möller, Z. Phys. D, **40**, 22 (1997)

[31] H. Heinze, P. Borrmann, H. Stamerjohanns and E. R. Hilf, Z. Phys. D, **40**, 190 (1997)

[32] Ph. Buffat and J.-P. Borel, Phys. Rev. A, **13**, 2287 (1976) )

[33] S. Iijima and T. Ichihashi, Phys. Rev. Lett. **56**, 616 (1986)

[34] H. Grönbeck, D. Tománek, S.G. Kim and A. Rosén, Chem. Phys. Lett. **264**, 39 (1997)

[35] S. Nosé, J. Chem. Phys. **81**, 511 (1984); W.G. Hoover, Phys. Rev. A, **31**, 1695 (1985)

[36] Bo Wästberg, "Calculations of Electronic Properties of Metal Clusters, Fullerenes and Molecules Adsorbed on Surfaces", Doctoral thesis, Chalmers University of Technology, Sweden (1992)

[37] Mats Andersson, "Metal Cluster Reactivity - Adsorption of Small Molecules in Bimolecular Collisions", Doctoral thesis, Chalmers University of Technology, Sweden (1995)

[38] Daniel Östling, "Electronic Structure and Optical Properties of $C_{60}$, Nanotubes and Carbon Onions", Doctoral thesis, Chalmers University of Technology, Sweden (1996)

[39] Henrik Grönbeck, "On the Structure of and Bonding in Metal Clusters", Doctoral thesis, Chalmers University of Technology, Sweden (1996)

[40] Lotta Holmgren, "Reactivity of metal clusters with diatomic molecules", Doctoral thesis, Chalmers University of Technology, Sweden (1998)

[41] Thorbjörn Åklint, "Construction of an experimental set-up for production and studies of deposited clusters", Licentiate thesis, Chalmers University of Technology, Sweden (1999)

[42] L. Holmgren, H. Grönbeck, Mats Andersson and A. Rosén, Phys. Rev. B, **53**, 16644 (1996).

[43] T. Dietz, M. Duncan, D. Powers and R. Smalley, J. Chem. Phys. **74**, 6511 (1981)

[44] V. Bondybey and J. English, J. Chem. Phys. **76**, 2165 (1982)

[45] M. Andersson, J. L. Persson, A. Rosén, J. Phys. Chem. **100**, 12222 (1996)

[46] J. B. Kaelberer and R. D. Etters, J. Chem. Phys. **66**, 3233 (1977)

[47] J. K. Lee, J. A. Barker and F. F. Abraham, J. Chem. Phys. **58**, 3166 (1973)

[48] R. S. Berry, T. L. Beck, H. L. Davis ans J. Jellinek, Adv. Chem. Phys. **52**, 75 (1988)

[49] P. Labastie and R. L. Whetten, Phys. Rev. Lett. **65**, 1567 (1990)

[50] H.-P. Cheng, X. Li, R. L. Whetten, and R. S. Berry, Phys. Rev. A **46**, 791 (1992)

[51] H. Hippler and J. Troe, "Advances in Gas Phase Photochemistry and Kinetics - Bimolecular Collisions", ed. by M. N. R. Ashfold and J. E. Baggott, The Royal Chemical Society, London (1989), p.209

[52] Andrew Zangwill, "Physics at surfaces", Cambridge University Press, Cambridge (1988)

[53] H. Schlichting, D. Menzel, T. Brunner and W. Brenig, Phys. Rev. Lett. **60**, 2515 (1988)

[54] F. A. Lindemann, Trans. Faraday Soc. **17**, 598 (1922)

[55] R. G. Gilbert, S. C. Smith, "Theory of Unimolecular Reactions", Blackwell Scientific Publixcations, Oxford (1990)

[56] K. Bolton, W. L. Hase, H. B. Schlegel and K. Song, Chem. Phys. Lett. **288**, 621 (1998)

[57] T. Yan and W. L. Hase, J. Phys. Chem. A, **105**, 2617 (2001)

[58] C. T. Rettner, D. J. Auerbach, J. C. Tully and A. W. Kleyn, J. Phys. Chem. **100**, 13021 (1996)

[59] B. Kasemo, Surf. Sci. **363**, 22 (1996)

[60] L. Sun, P. de Sainte Clare, O. Meroueh and W. L. Hase, J. Chem. Phys. **114**, 535 (2001)

[61] C. Åkerlund, I. Zoric and B. Kasemo, Surf. Sci. **418**, 543 (1998)

[62] S. Fedrigo, W. Harbich and J. Buttet, Phys. Rev. B, **58**, 7428 (1998)

[63] R. Neuendorf, R. E. Palmer, R. Smith, App. Phys. Lett. **77**, 3003 (2000)

[64] U. Even, J. Schek and J. Jortner, Chem. Phys. Lett. **202**, 303 (1993)

[65] U. Even, P. J. de Lange, H. Th. Jonkmann and J. Kommandeur, Phys. Rev. Lett. **56**, 965 (1986)

[66] K. Tögelhofer, F. Aumayr, H. Kurz, H. P. Winter, P. Scheier and T. D. Märk, J. Chem. Phys. **99**, 8254 (1993)

[67] R. C. Mowrey, D. W. Brenner, B. I. Dunlap, J. W. Mintmire and C. T. White, J. Phys. Chem. **95**, 7138 (1993)

[68] H. Yasumatsu, U. Kalmbach, S. Koizumi, A. Terasaik and T. Kondow, Z. Phys. D, **40**, 51 (1997)

[69] H. Haberland, Z. Insepov and M. Moseler, Phys. Rev. B, **51**, 11061 (1995)

[70] H.-P. Cheng and U. Landmann, Science, **260**, 1304 (1993)

[71] G.-Q. Xu, S. L. Beransek and J. C. Tully, J. Chem. Phys. **88**, 3376 (1988)

[72] Eur. Phys. J. D, **9** (1999)

[73] W. Christen and U. Even, Eur. Phys. J. D. **9**, 29 (1999)

[74] P. U. Andersson and J. B. C. Pettersson, Z. Phys. D **41**, 57 (1997)

[75] L. Ming, M. Svanberg, N. Markovic, and J. B. C. Petterson, J. Phys. Chem. **101**, 4011 (1997)

[76] D. Greenspan and L. F. Heath, J. Phys. D, Appli. Phys, **24**, 2121 (1991)

[77] J. Schulte, R. R. Lucchese and W. H. Marlow, J. Chem. Phys. **99**, 1178 (1993)

[78] P. de Saint Clarie and W. L. Hase, J. Phys. Chem. **100**, 8190 (1996)

[79] P. de Saint Clarie, G. H. Peslherbe and W. L. Hase, J. Phys. Chem. **99**, 8147 (1995)

[80] D. C. Tardy and B. S. Rabinovitch, Chem. Rev. **77**, 396 (1977)

[81] "Les Prix Nobel", Almqvist & Wiksell international, Stockholm, 1986

[82] S. Nonose, H. Tanaka, T. Mizuno, F. Ishizaka and T. Kondow, Z. Phys. D, **40**, 75 (1997)

[83] J. M. Millam, V. Bakken, W. Chen, W. L. Hase and H. B. Schlegel, J. Chem. Phys. **111**, 3800 (1999)

[84] C. N. Hinshelwood, Proc. Roy. Soc. (A), **113**, 230 (1927)

[85] D. C. Tardy and B. S. Rabinovitch, J. Chem. Phys. **45**, 3720 (1966)

[86] S. Nordholm, B. C. Freasier and D. Jolly, Chem. Phys. **25**, 433 (1977)

[87] L. E. B. Börjesson and S. Nordholm, Chem. Phys. **212**, 393 (1996)

[88] L. E. B. Börjesson, L. Ming and S. Nordholm, Chem. Phys. **221**, 253 (1997)

[89] D.Tománek, S.Mukherjee and K. H. Bennemann, Phys. Rev. B, **28**, 665 (1983); W. Zhong, Y. S. Li and D. Tománek, Phys. Rev. B, **44**, 13053 (1991)

[90] R. P. Gupta, Phys, Rev. B, **23**, 6265 (1980)

[91] G. K. Wertheim, S. B. DiCenzo and D. N. E. Buchanan, Phys, Rev. B, **33**, 5384 (1986)

[92] G. L. Estiú and M. C. Zerner, J. Phys. Chem. **98**, 4793 (1994)

[93] F. Cleri and V. Rosato, Phys. Rev. B, **48**, 22 (1993)

[94] C. Rey, L. J. Gallego, J. García-Rodeja, J. A. Alonso and M. P. Iñiguez, Phys. Rev. B, **48**, 8253 (1993)

[95] X. Chen, J. Zhao, Q. Sun, F. Liu, G. Wang and X. Shen, Phys. Stat. Sol. (b), **193**, 355 (1996)

[96] M. S. Daw, Phys. Rev. B, **39**, 7441 (1989); M. S. Daw and M. I. Baskes, Phys. Rev. B, **29**, 6443 (1984)

[97] K. W. Jacobsen, J. K. Nörskov and M. J. Puska, Phys. Rev. B, **35**, 7423 (1987)

[98] M. Jarrold and J. E. Bower, J. Chem. Phys. **87**, 5737 (1987)

[99] C. Kittel, "Introduction to Solid State Physics", John Wiley & Sons, New York (1986)

[100] M. Morse, Chem. Rev. **86**, 1074 (1986)

[101] Y. S. Touloukian, R. K. Kirby, R. E. Taylor and P. D. Desai, "Thermophysical properties of matter", vol. 12, IFI/PLENUM, New York (1977)

[102] O. Echt, K. Sattler and E. Recknagel, Phys. Rev. Lett, **47**, 1121 (1981)

[103] A. L. Mackay, Acta Crystal. **15**, 916 (1962)

[104] P. M. Ajayan and L. D. Marks, Phys. Rev. Lett. **60**, 585 (1988)

[105] C. J. Tsai and K. D. Jordan, J. Phys. Chem. **97**, 11227 (1993)

[106] H. B. Callen, "Thermodynamics and an introduciton to thermostatics", John Wiley & sons (1985)

[107] P. W. Atkins, "Physical Chemistry", 3rd edition, Oxford University Press, Oxford (1986)

[108] D. J. Wales, Mol. Phys. **78**, 151 (1993)

[109] T. Hill, Thermodynamics of Small Systems, Benjamin, New York, pt. I, 1963; pt. II 1964

[110] R. S. Berry, J. Jellinek and G. Natanson, Chem. Phys. Lett. **107**, 227 (1984)

[111] R. S. Berry, J. Jellinek and G. Natanson, Phys. Rev. A, **30**, 919 (1984)

[112] Y. Imry, Phys. Rev. B, **21**, 2042 (1980)

[113] F. Amar and R. S. Berry, J. Chem. Phys. **85**, 5943 (1986)

[114] F. A. Lindemann, Physik Z. **11**, 609 (1910)

[115] M. Moseler and J. Nordiek, Phys. Rev. B, **60**, 11734 (1999)

[116] F. H. Stillinger and T. A. Weber, J. Chem. Phys. **81**, 5089 (1984)

[117] J. P. K. Doye and D. J. Wales, J. Chem. Phys. **102**, 9659 (1995)

[118] A. Proykova and R. S. Berry, Z. Phys. D, **40**, 215 (1997)

[119] H.-P. Cheng and R. S. Berry, Phys. Rev. A, **45**, 7969 (1992)

[120] J. P. K. Doye and D. J. Wales, Z. Phys. D, **40**, 466 (1997)

[121] R. Kjellander, "The basis of statistical thermodynamics", Göteborg University (1991)

[122] S. M. Thompson, K. E. Gubbins, J. P. R. B. Walton, R. A. R. Chantry and J. S. Rowlinson, J. Chem. Phys. **81**, 530 (1984)

[123] D. Frenkel and B. Smit, "Understanding Molecular Simulation", Academic Press, San Diego, (1996)

[124] E. S. Severin, B. C. Freasier, N. D. Hamer, D. L. Jolly ans S. Nordholm, Chem. Phys. Lett. **57**, 117 (1978)

[125] H. W. Schranz, S. Nordholm and G. Nyman, J. Chem. Phys. **94**, 1487 (1990)

[126] N. Metropolis, A. W. Rosenbluth, M. N. Rosenbluth, A. H. Teller and E. Teller, J. Chem. Phys. **21**, 1087 (1953)

[127] L. Ming, S. Nordholm and H. Schranz, Chem. Phys. Lett. **248**, 228 (1996)

[128] http://fy.chalmers.se/f3c/MonteLab.htm

[129] S. Valkealahti and M. Manninen, Z. Phys. D, **26**, 255 (1993)

[130] T. P. Martin, U. Näher, H. Schaber and U. Zimmermann, J. Chem. Phys. **100**, 2322 (1994)

[131] D. J. Shaw, "Introduction to Colloid and Surface Chemistry, Butterworth-Heinemann", Oxford (1992), p. 64

[132] D. Y. Sun and X. G. Gong, Phys. Rev. B, **57**, 4730 (1998)

[133] T. L. Beck and R. S. Berry, J. Chem. Phys. **88**, 3910 (1988)

[134] J. P. K. Doye and D. J. Wales, J. Chem. Phys. **102**, 9673 (1995)

[135] A. B. Belonoshko, Geochim. Cosmochim. Acta, **58**, 4039 (1994); A. B. Belonoshko and L. S. Dubrovinsky, Am. Mineral, **81,** 303 (1996); R. Ahuja, A. B. Belonoshko and B. Johansson, Phys. Rev. E, **57**, 1673 (1998); A. B. Belonoshko, Phys. Chem. Minerals, **25**, 138 (1998)

[136] J. D. Kubicki and A. C. Lasaga, Amer. J. Sci. **292**, 153 (1992)

[137] J. Westergren, S. Nordholm and R. Penfold, Mol. Sim. **27**, 17 (2001)

[138] C. L. Cleveland, W. D. Luedtke and U. Landmann, Phys. Rev. Lett. **81**, 2036 (1998)

[139] H.-X. Zhou and R. Zwanzig, J.Chem. Phys. **94**, 6147 (1991); R. Zwanzig, J. Chem. Phys. **97**, 3587 (1992)

[140] S. F. Chekmarev and S. V. Krivov, Eur. Phys. J. D, 9, 204, Chem Phys. Lett. **287**, 719 (1998)

[141] D. D. Frantz, J. Chem. Phys. **102**, 3747 (1995)

[142] F. Calvo and F. Spiegelmann, J. Chem. Phys. **112**, 2888 (1999)

[143] J. P. Neirotti, F. Calvo, D. L. Freeman and J. D. Doll, J. Chem. Phys. **112**, 10340 (2000)

[144] L. M. Amon and W. P. Reinhardt, J. Chem. Phys. **113**, 3573 (2000)

[145] F. Calvo and P. Labastie, Chem. Phys. Lett. **247**, 395 (1995)

[146] R. Potaeu, F. Spiegelmann and P. Labstie, Z. Physik D, **30**, 57 (1994)

[147] A. Münster, Statistical Thermodynamics vol. 2, (Springer Verlag, Berlin 1974), p. 582

[148] M. Svanberg and J. B. C. Pettersson, Chem. Phys. Lett. **263**, 661 (1996)

[149] W. H. Press, S. A. Teukolsky, W. T. Vetterling and B. P. Flannery, Numerical Recipies (Cambridge University Press, Cambridge, 1992)

[150] L. Ming, J. Davidsson and S. Nordholm, J. Chem. Phys. **104**, 9001 (1996)

[151] L. E. B. Börjesson, J. Davidsson, N. Markovic and S. Nordholm, Chem. Phys. **177**, 133 (1993)

[152] H. Svedung, N. Markovic and S. Nordholm Chem Phys. **248**, 195 (1999)

[153] S. Nordholm, L. E. B. Börjesson, L. Ming and H. Svedung, Ber. Bunsenges. Phys. Chem. **101**, 574 (1997)

[154] M. Head-Gordon, J. C. Tully, C. T. Rettner, C. B. Mullins and D. J. Auerbach, J. Chem. Phys. **94**, 1516 (1991)

[155] M. Andersson, L. Holmgren and A. Rosén, Surf. Rev. Lett. **3**, 683 (1996)

[156] D. E. Oner, R. Chakarova, I. Zoric and B. Kasemo, J. Chem. Phys. **113**, 8869 (2000)

[157] B. Baule, Ann. Phys. **44**, 145 (1914)

[158] D. Tomanek, Z. Sun, S. G. Louie, Phys. Rev. B, **43**, 4699 (1991)

[159] H. Grönbeck, A. Rosén and W. Andreoni, Z. Phys. D, **40**,206 (1997)

[160] H. Grönbeck and A. Rosén, Chem. Phys. Lett. **227**, 149 (1994)

[161] G. Lendvay and G. Schatz, J. Phys. Chem. **96**, 3752 (1992)

[162] H. Svedung, L. E. B. Börjesson, N. Markovic and S. Nordholm Chem Phys. **236**, 189 (1998)

[163] L. E. B. Börjesson and S. Nordholm, J. Phys. Chem. **99**, 938 (1995)

[164] T. Brunner and W. Brenig, Surf. Science, **291**, 192 (1993)

[165] U. Frenzel, U. Hammer, H. Westje and D. Kreisle, Z. Phys. D, **40**, 108

[166] A. Rytkönen, H. Häkkinen and M. Manninen, Eur. Phys. J. D, **9**, 451 (1999)